Article
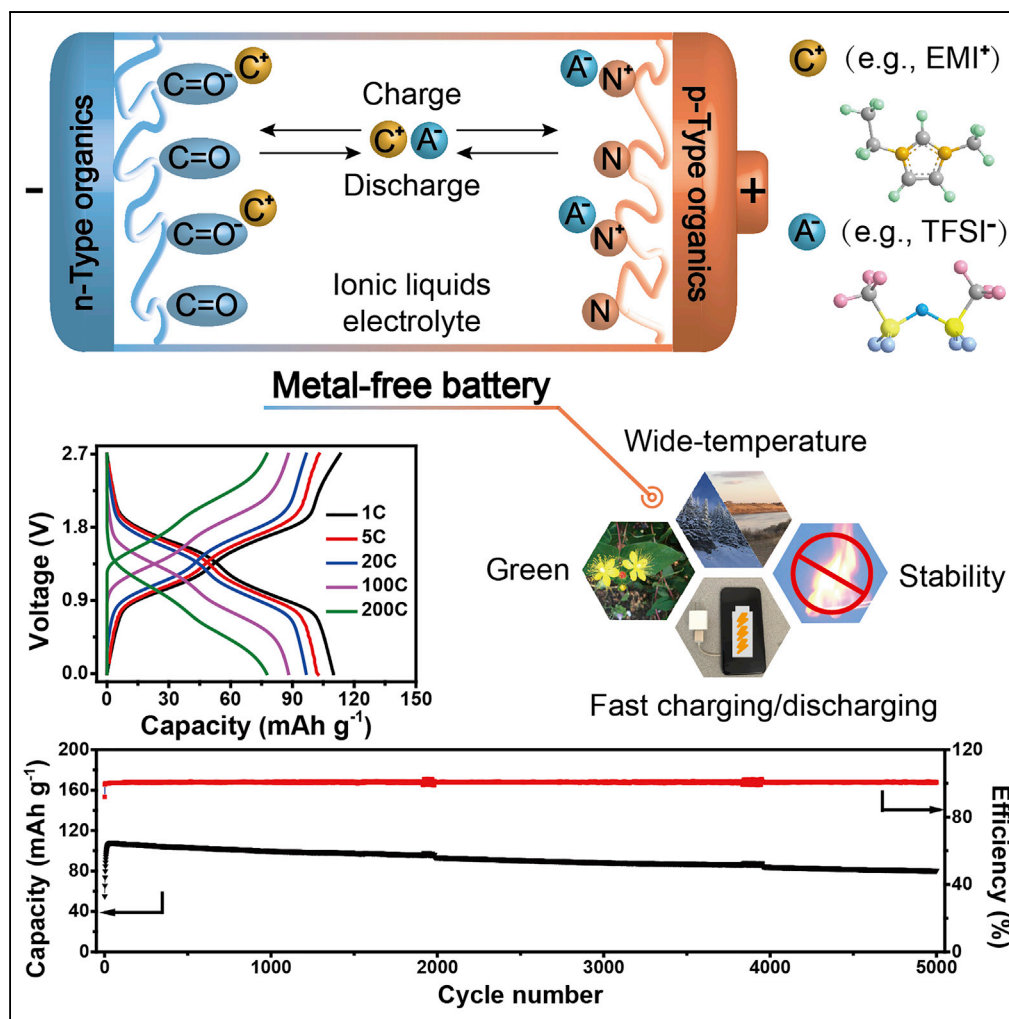
A Metal-free Battery with Pure Ionic Liquid Electrolyte

Jian Qin, Qing Lan, Ning Liu, Fang Men, Xin Wang, Zhiping Song, Hui Zhan

zpsong@whu.edu.cn (Z.S.)
zhanhui3620@126.com (H.Z.)

HIGHLIGHTS

Metal-free battery was demonstrated by PI5/EMITFSI/PTPAn cell

Organic cation/anion storage was realized

Ionic liquid was used alone as electrolyte and acted as the cation/anion supplier

PI5/EMITFSI/PTPAn cell exhibited superstable cycling and remarkable rate capability

Article

A Metal-free Battery
with Pure Ionic Liquid Electrolyte

Jian Qin,[1] Qing Lan,[1] Ning Liu,[1] Fang Men,[1] Xin Wang,[1] Zhiping Song,[1,2,*] and Hui Zhan[1,3,4,*]

SUMMARY

Metal or metal-ion-based batteries represent the mainstream battery technology, in which metal ions either participate in the electrode redox reaction or act as the charge carrier in the electrolyte. The principle guides battery designs and leads to the most widely adopted battery construction of metal-ion acceptor/metal salt in solvent/metal-ion donor. Although these architectures have seen significant progress, there are still many issues with them, including dendrite growth, solid-electrolyte interface corruption, and safety concerns. In this article, the intercalation/deintercalation of organic cations other than metal ions is explored in an all-organic battery composed of organic anode/cathode and pure ionic liquid electrolyte. This metal-free and solvent-free concept has been demonstrated by polyimide/1-ethyl-3-methylimidazolium bis(trifluoromethylsulfonyl)imide/polytriphenylamine full-cell, through which capacity near theoretical value, more than 5,000 cycling life, rate capability up to 200 C, and remarkable low-temperature performance has been achieved. Our work provides an alternate way of developing future efficient, safe, green, and versatile batteries.

INTRODUCTION

Over the past decades, we are seeing the biggest changes in energy storage industry, in which renewable energy has a rising role and has earned increased attention. Electrochemical energy storage and conversion, especially batteries, as an important member in the emerging energy field, made tremendous progress (Nitta et al., 2015; Larcher and Tarascon, 2015; Van Noorden, 2014). From the early lead-acid, nickel-cadmium, and nickel-hydrogen batteries, to the current lithium, sodium (Slater et al., 2013), and magnesium batteries (Muldoon et al., 2014), a variety of batteries have been developed, with different charge/discharge mechanisms and anode/electrolyte/cathode constructions summarized in Figure 1A. Among them, aprotic metal battery (e.g., Li/S and Li/air, Bruce et al., 2012) and aprotic metal-ion battery (e.g., graphite/$LiCoO_2$ and hard carbon/$Na_3V_2(PO4)_3$, Rui et al., 2015) undoubtedly are the mainstream of current research. In addition, aqueous metal-ion battery (e.g., polyimide (PI)/$LiNO_3$/$LiCoO_2$, Qin et al., 2014) has become increasingly attractive in recent years owing to its prominent safety and potential application in grid energy. The above-mentioned batteries have one thing in common that metal cation (M^+) is the only charge carrier in ion conduction and charge balancer in electrode redox. Beside this typical battery concept, the battery involving metal cation (M^+) participating in the anode reaction and anion (A^-) participating in the cathode reaction was proposed recently, and typical examples are dual-graphite battery (also called *dual-ion battery* by some authors, Read et al., 2014; Fan et al., 2017) and all-organic battery (e.g., poly(anthraquinonyl sulfide) (PAQS)/polytriphenylamine (PTPAn), Deng et al., 2013, and PI/PTPAn, Dong et al., 2018). All the above-mentioned batteries, with either inorganic or organic electrode materials, have two indispensable components. One is the metal element (e.g., Li, Na, K, Mg); apart from being a major participant in anode electrochemical redox (e.g., Li^+/Li, Mg^{2+}/Mg, …), it is also an important charge carrier within the electrolyte or electrode material. The other is the solvent (either aprotic ester and ether or water) in the electrolyte, which functions as the medium dissolving the electrolyte salt and maintaining ionic conductivity. However, these two primary components bring some issues, such as unforeseen metal dendrite growth, volatility and flammability of aprotic solvent, and less reliable stability of electrolyte toward electrode. In addition, the annoying solid-electrolyte interface (SEI) issues and even concerns on metal resource can be generated. All these hamper the further improvement and practical application of existing battery systems.

Actually, current research already provides some clues to the solution. On one hand, organic electrode materials (Liang et al., 2012, Liang and Yao, 2018; Schon et al., 2016; Song and Zhou, 2013) can help to wean from the dependence on transition metal-based inorganic electrode and provide more space on performance improvement. Generally, the organic electrode materials can be divided into n-type (reduced to

[1]Hubei Key Lab of Electrochemical Power Sources, College of Chemistry and Molecular Sciences, Wuhan University, Wuhan 430072, China
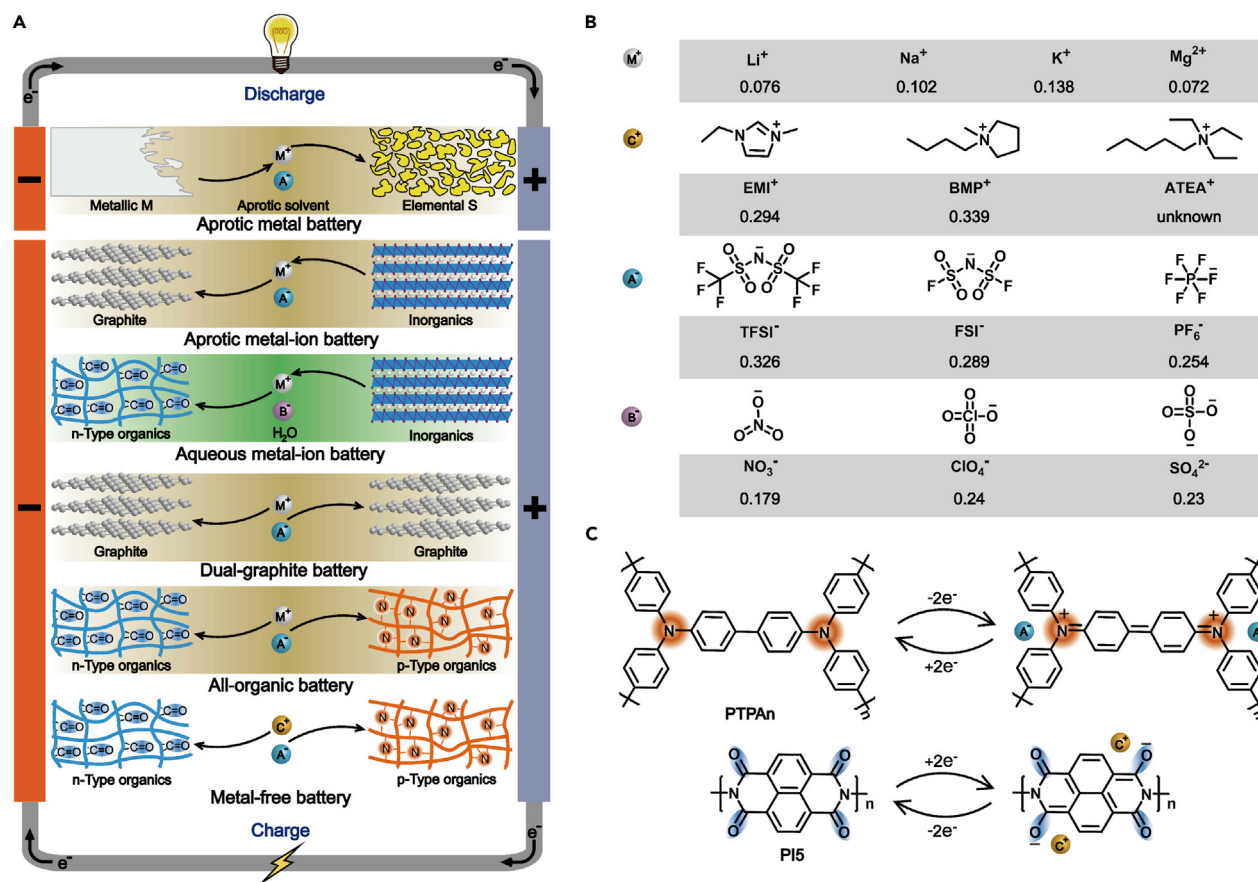
[2]Key Laboratory of Advanced Energy Materials Chemistry (Ministry of Education), Nankai University, Tianjin 300071, China

[3]Engineering Research Center of Organosilicon Compounds & Materials, Ministry of Education, Wuhan University, Wuhan 430072, China

[4]Lead Contact

*Correspondence:
zpsong@whu.edu.cn (Z.S.),
zhanhui3620@126.com (H.Z.)
https://doi.org/10.1016/j.isci.2019.04.010

Figure 1. Cell Configurations and Related Information of Various Rechargeable Batteries

(A) The cell configurations and charge transfer processes of five conventional rechargeable batteries, including aprotic metal battery, aprotic metal-ion battery, aqueous metal-ion battery, dual-graphite battery, and all-organic battery, and the totally metal-free battery proposed in this work. For electrode materials, M means alkali or alkaline earth metal such as Li, Na, K, or Mg; inorganics are intercalation materials represented by the transition metal oxide as $LiCoO_2$, $LiFePO_4$, etc.; n-type organics are mostly carbonyl polymers, such as polyimides (e.g., PI5) and quinone polymers; p-type organics are usually conjugated amine-based polymers such as polytriphenylamine (PTPAn). For electrolytes, the brown color represents conventional, non-aqueous electrolyte consisting of aprotic solvent, metal cation M^+, and anion A^- such as bis(trifluoromethylsulfonyl)imide ($TFSI^-$), bis(fluorosulfonyl)imide (FSI^-), and hexafluorophosphate (PF_6^-); the green color represents aqueous electrolyte consisting of H_2O, M^+, and anion B^- such as NO_3^-, ClO_4^-, and SO_4^{2-}. The novel solvent-free electrolyte only contains pure ionic liquid, typically composed of anion A^- and organic cation C^+ such as 1-ethyl-3-methylimidazolium (EMI^+), 1-butyl-1-methylpyrrolidinium (BMP^+), and amyltriethylammonium ($ATEA^+$).

(B) The structure and ionic radius (in nm) (Yabuuchi et al., 2014; Hong et al., 2014; Tokuda et al., 2004; Hu et al., 2014; Gloe et al., 2003) of the aforementioned cations (M^+ and C^+) and anions (A^- and B^-).

(C) Electrochemical redox mechanism of the metal-free battery illustrated by PI5/pure ionic liquid/PTPAn full-cell.

negatively charged species and neutralized by receiving cations) and p-type (oxidized to positively charged species and neutralized by receiving anion) and applied as anode or cathode in various battery types (Figure 1A) (Song and Zhou, 2013). Within the n-type family, carbonyl-based organics such as quinone polymers and polyimides, have been widely studied and have demonstrated high capacity and reliable stability. More importantly, owing to its unique cation-independent redox character, this type of organics, for example, PAQS (Song et al., 2009; Zhang et al., 2017; Jian et al., 2016; Bitenc et al., 2015), is capable of reacting with different metal cations including Li^+, Na^+, K^+, and Mg^{2+} without crystalline limitation. On the other hand, in the last few years, the safety advantage of room-temperature ionic liquid (Armand et al., 2009a, MacFarlane et al., 2016) has been extensively reported and its application in battery has been frequently mentioned, because of the merits of non-volatility, non-flammability, as well as chemical, electrochemical, and thermal stabilities. Other than improving battery safety (Guerfi et al., 2010), its effect in regulating the electrode/electrolyte interface (Piper et al., 2015) and suppressing the dissolution and shuttle of sulfur cathode has also been revealed (Wang et al., 2016). Nevertheless, when using ionic liquid, there

is usually a tradeoff between the viscosity, ionic conductivity, and safety. Hence, in practical case, adding aprotic solvent to form binary, ternary, and even quaternary electrolyte is necessary, and then it certainly reduces the advantage of ionic liquid. Virtually, the ionic conductivity of many pure ionic liquids fully satisfies the requirement of rechargeable batteries ($>10^{-3}$ S cm^{-1} at room temperature) (Hao et al., 2011); it alone can well fulfill the ion transfer within the electrolyte, and then single-component electrolyte totally composed of ionic liquid is feasible. Unfortunately, the current battery designs all required metal ion as charge carriers, which is absent in pure ionic liquid. Up to today, reversible organic cation (C$^+$) intercalation/de-intercalation into electrode material has been hardly reported. The pioneer work attempting to use pure ionic liquid electrolyte in dual-graphite battery was not that successful (Fan et al., 2017); the results as well as many other literatures (Lu et al., 2009; Fu et al., 2009) indicated that graphite was not an appropriate anode for C$^+$ intercalation because it will be gradually exfoliated by the large C$^+$, leading to low cycling stability and low coulombic efficiency.

Herein, for the first time, we discovered that n-type organic electrode materials showed unique redox reversibility with organic cation (C$^+$) in ionic liquid, and thus realized a novel, totally metal-free and solvent-free battery construction by n-type organic anode, p-type organic cathode, and pure ionic liquid electrolyte. It was different from previously reported batteries by the real metal-free character and organic-cation-based redox reaction. The pure ionic liquid electrolyte makes the battery intrinsically safe, whereas the solvent-free electrolyte together with the all-organic electrode design well resolves the issues produced by solvation effect or the unwanted interaction between solvent and electrode, and further supplies a possible new strategy for energy density improvement. In addition, the metal-free character enhances the battery's resource sustainability and environment friendliness and simplifies battery disposal. In this article, the battery was mainly demonstrated by the full-cell composed of polyimide (PI5) anode, PTPAn cathode, and 1-ethyl-3-methylimidazolium bis(trifluoromethylsulfonyl)imide (EMITFSI) electrolyte (Figure 1C). The PI5/EMITFSI/PTPAn full-cell exhibited superfast reaction kinetics, capacity close to 111 mAh g^{-1} based on PTPAn, and very stable cycling performance. In addition, it showed distinctive temperature adaptability and promising application in wide-temperature-range operation. We believe the metal-free battery proposed in this work provides fresh idea beyond existing battery types, toward future efficient, safe, green, sustainable, and versatile energy storage.

RESULTS

Material Selection and Half-Cell Performance

To construct the metal-free battery, appropriate n-type organic anode, p-type organic cathode, and pure ionic liquid electrolyte need to be selected first. Although many organic electrode materials had been studied before, only a few polymers showed reliable redox reversibility and cycling stability. We scanned the literatures (Song and Zhou, 2013) and summarized the candidate pool in Figure S1. The n-type anode could include polyimide (PI2 and PI5) and polyanthraquinone (PAQ), possessing relatively high specific capacity (200–300 mAh g^{-1}) and low redox potential (2.0–2.7 V versus Li$^+$/Li); the p-type cathode could be PTPAn (Figure S2), polyaniline, and poly(2,2,6,6-tetramethylpiperidine-1-oxyl-4-yl methacrylate), with relatively low specific capacity (100–150 mAh g^{-1}) and high redox potential (3.0–4.0 V versus Li$^+$/Li). After considering the cycling stability, cell voltage, and capacity, PI5 was chosen as the anode, whereas PTPAn was used as the cathode. On the other hand, we mainly focused on ionic liquids with bis(trifluoromethylsulfonyl)imide (TFSI$^-$) anion owing to their low viscosity and high conductivity feature (TFSI$^-$ salt usually had higher ionic conductivity than hexafluorophosphate (PF$_6^-$) and lower melting point than BF$_4^-$ series; Hao et al., 2011; Garcia et al., 2004). Among the analogs, imidazole ionic liquid of EMITFSI was finally picked because 1-ethyl-3-methylimidazolium (EMI$^+$) had lower viscosity of 38.1 cP and smaller ionic radius than 1-butyl-1-methylpyrrolidinium (BMP$^+$) and amyltriethylammonium (ATEA$^+$) (Figure 1B) and its easy preparation, purification, and storage meant potential future low price (among the ionic liquids, EMITFSI has characteristics of easy preparation and easy purification because of the relatively smaller molecule and simpler molecular structure, and compared with many other lithium salts, its much less reactivity toward water may lead to easier production and storage). However, in the later, BMPTFSI and ATEATFSI were still used to demonstrate the universality of the metal-free battery.

Before testing the full-cell performance, it was necessary to investigate the electrochemical behavior of PI5 anode and PTPAn cathode separately in EMITFSI electrolyte, because it was a brand new electrolyte for rechargeable batteries. To accurately measure the potential of PI5 and PTPAn in EMITFSI electrolyte, a three-electrode cell was used in either galvanostatic charge/discharge test or cyclic voltammogram (CV)
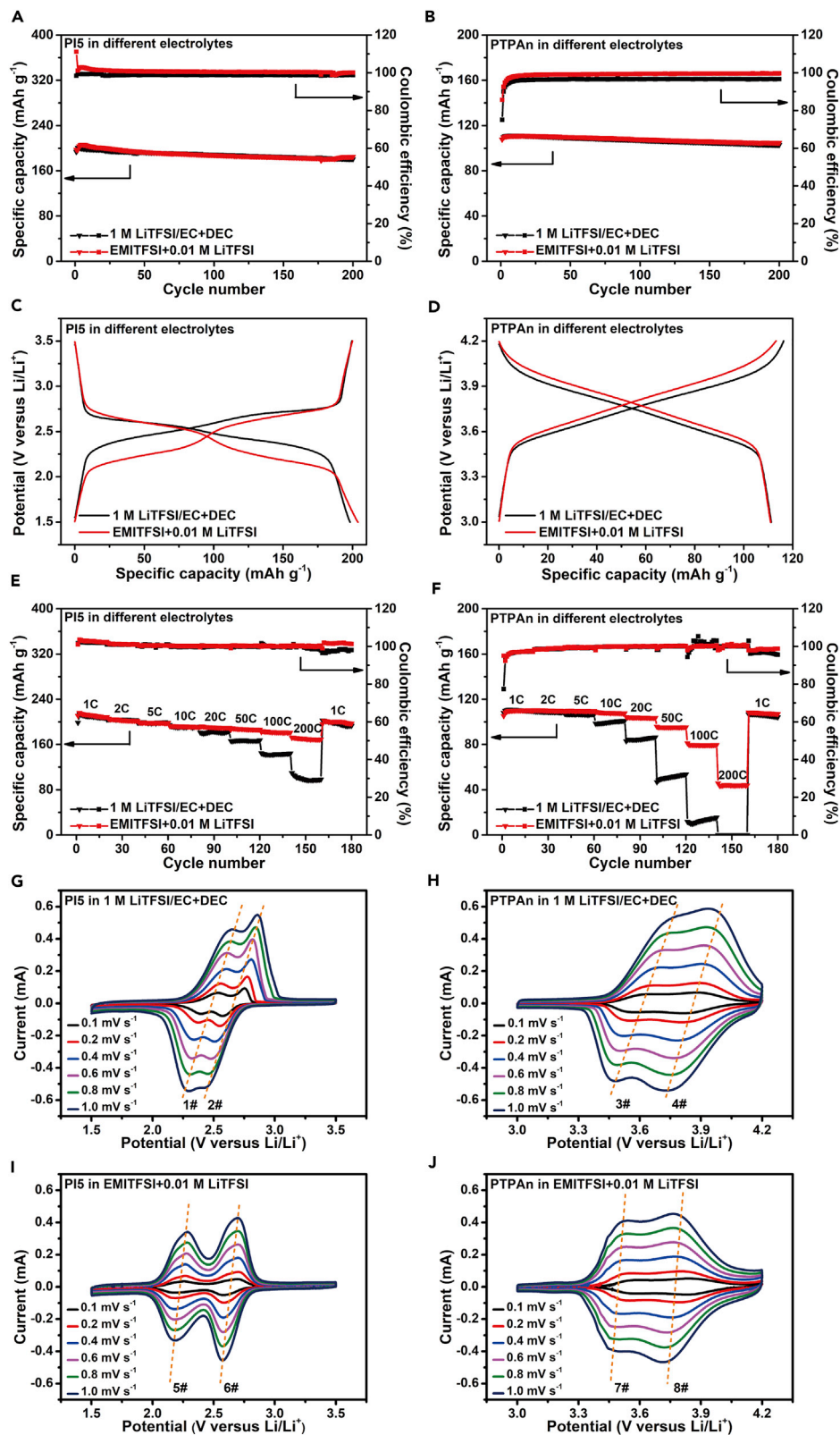
Figure 2. Comparison of PI5 and PTPAn Electrode in Conventional Ester Electrolyte and Novel Ionic Liquid Electrolyte

(A and B) The cycling performance of (A) PI5 and (B) PTPAn at 1 C rate in 1 M LiTFSI/EC + DEC electrolyte (viscosity: 4.51 cP) and EMITFSI + 0.01 M LiTFSI electrolyte (viscosity: 41.1 cP) (0.01 M LiTFSI was added into pure ionic liquid to establish the Li$^+$/Li redox couple on Li reference electrode, see the Methods part).

(C and D) The typical voltage profiles (from the 10th cycle) of (C) PI5 and (D) PTPAn in the two electrolytes.

(E and F) The rate performance of (E) PI5 and (F) PTPAn in the two electrolytes; the current rate changed in stepwise mode from 1 C to 200 C.

(G–J) The typical CV curves of (G and I) PI5 and (H and J) PTPAn in the two electrolytes at different scan rates from 0.1 mV s^{-1} to 1 mV s^{-1}. Corresponding data analysis of the redox peaks labeled from 1# to 8# could be found in Figure S6.

test. PI5 was the working electrode, whereas excess PTPAn was the counterelectrode, and vice versa if PTPAn was studied. Li foil was used as the quasi-reference electrode for both of them, and 0.01 M LiTFSI was added into EMITFSI to establish a Li$^+$/Li redox couple, leading to 0.12 V lower potential than standard Li$^+$/Li potential according to Nernst equation (see the method part). The possible competing reaction between EMI$^+$ and Li$^+$ with the n-type PI5 electrode barely happened due to the very low Li$^+$/EMI$^+$ molar ratio (1/391). For convenience, EMITFSI electrolyte is hereinafter referred to as EMITFSI + 0.01 M LiTFSI for half-cell and pure EMITFSI for full-cell.

The results of galvanostatic charge/discharge test of PI5 and PTPAn in EMITFSI electrolyte and 1 M LiTFSI/ethylene carbonate (EC) + diethyl carbonate (DEC) electrolyte was compared in Figures 2A–2D (results in 1 M LiPF$_6$/EC + DEC were presented in Figure S3). Generally, in either electrolytes, PI5 and PTPAn showed quite similar capacity and cycling performance (Figures 2A and 2B). They all exhibited high redox reversibility with maximum capacity of 206 mAh g^{-1} (PI) and 111 mAh g^{-1} (PTPAn) and stable cycling with little capacity fading during 200 cycles (10% for PI5 and 5.7% for PTPAn, respectively). If comparing with 1 M LiTFSI/EC + DEC electrolyte, EMITFSI electrolyte actually brought even higher coulombic efficiency (stable value of 98.6%–100.0% for PI5 and 96.5%–99.6% for PTPAn). Moreover, for PI5 anode, lower average charge voltage was obtained in EMITFSI electrolyte (2.46 V) than in 1 M LiTFSI/EC + DEC (2.58 V, Figure 2C), whereas for PTPAn cathode, little higher average discharge voltage (from 3.74 to 3.77 V, Figure 2D) was observed in EMITFSI electrolyte. The difference in charge and discharge voltages together implied higher working voltage of PI5/PTPAn full-cell with EMITFSI electrolyte (Figure S4).

The rate capability of the organic electrode was examined. Previously, ionic liquid electrolyte was usually criticized for increasing the viscosity, decreasing the ionic conductivity of the electrolyte, and further harming the high-rate performance (Garcia et al., 2004). The result of charge/discharge tests under stepwise increasing current was shown in Figures 2E and 2F. PI5 and PTPAn both presented much superior rate capability in EMITFSI electrolyte than in 1 M LiTFSI/EC + DEC electrolyte. For instance, under 200 C, the capacity of PI5 in EMITFSI electrolyte (84% retention) almost doubled that in 1 M LiTFSI/EC + DEC (48% retention); for PTPAn, the 40% capacity retention at 200 C was achieved in EMITFSI electrolyte; and it mostly could not work in 1 M LiTFSI/EC + DEC. A similar trend was revealed in CV measurements (Figures 2G–2J and S5). When the scan rate was increased from 0.1 to 10 mV s^{-1} (PI5) or 0.1 to 6 mV s^{-1} (PTPAn), highly symmetrical redox peaks were preserved in EMITFSI, whereas in 1 M LiTFSI/EC + DEC, the cathodic branches leaned to more negative voltage and the anodic ones leaned to more positive voltage, agreeing with previous reports (Feng et al., 2008; Song et al., 2010). The results suggested much better redox reversibility of PI5 and PTPAn in EMITFSI.

We tried to semi-quantitatively compare the electrochemical behavior of PI5 and PTPAn in different electrolytes. Either in EMITFSI or 1M LiTFSI/EC + DEC electrolyte, the dependence of peak current (i) on scan rate (v) followed the power law equation of $i = av^b$, in which b could be indicative of the surface-controlled reaction ($b = 1$) or the bulk diffusion-controlled reaction ($b = 0.5$) (Augustyn et al., 2013; Jung et al., 2017). The data analysis in Figure S6 showed that the b values for PI5 were significantly increased from 0.77–0.93 range in 1 M LiTFSI/EC + DEC to 0.95–0.99 in EMITFSI, whereas for PTPAn, they were slightly increased from 0.94–0.98 to 0.95–0.99. The b values of PI5 and PTPAn all being close to 1 in EMITFSI electrolyte indicated that they mostly undergo a pseudocapacitive reaction, which might be the reason for the excellent high-rate performance and the faster reaction kinetics of PI5 and PTPAn in EMITFSI electrolyte. We thought the different electrochemical kinetics could be explained by the high ionic conductivity as well as the non-solvation nature of ionic liquid. EMITFSI electrolyte showed higher ionic conductivity (10.8 mS cm^{-1}, consistent with the reported value, Garcia et al., 2004) than 1 M LiTFSI/EC + DEC (7.4 mS cm^{-1}) at room

temperature (Figure S7). It was unexpected but still reasonable if the following points were taken into account. First, the highly ionized and solvent-free feature of EMITFSI could bring more available ion conduction carriers (EMI$^+$/Li$^+$ = TFSI$^-$ [in pure EMITFSI]/TFSI$^-$ [in 1 M LiTFSI/EC + DEC] = 3.9/1) in per unit volume of electrolyte; second, the much bigger ionic size of EMI$^+$ (0.294 nm) than Li$^+$ (0.076 nm) greatly weakened the coordination with solvent and the electrostatic interaction with anion (TFSI$^-$), and it could be evidenced by a supplementary test, in which the diluent electrolytes of 0.1 M EMITFSI/EC + DEC still showed higher conductivity than 0.1 M LiTFSI/EC + DEC (Figure S7). Beside the ionic conductivity, the solvation effect might be another important factor affecting the reaction kinetics, which was rarely emphasized in the study of inorganic electrode materials due to the rate-controlling step of ion diffusion within the lattice (Levin et al., 2017). However, because the electrochemical reaction of organic electrode material, like PI5, was pseudocapacitive in principle, it could be benefitted by the faster transportation of non-solvated EMI$^+$, absence of solvation/de-solvation process, as well as the higher cation abundance. EMITFSI promoting the rate performance of PTPAn could be explained similarly. Despite the same doping anion of TFSI$^-$ in the two different electrolytes, the higher TFSI$^-$ concentration and weaker interaction within EMI$^+$–TFSI$^-$ ion pair guarantee immediate TFSI$^-$ supply for the p-type reaction. In summary, ionic liquid electrolyte not only participates in the electrochemical redox of n-type anode and p-type cathode but also endows the ultrafast reaction kinetics of the metal-free battery.

Full-Cell Performance and Analysis

Hereinabove, the electrochemical property of PI5 and PTPAn was well investigated and their superior electrochemical property in EMITFSI electrolyte was revealed; next the PI5/PTPAn full-cell was examined. In the galvanostatic charge/discharge tests of the full-cell, the C rate and specific capacity were all based on the cathode. Figures 3A and 3B showed the cycling behavior and voltage profiles under 1 C rate, in which the specific capacity reached 111 mAh g^{-1} in 10 cycles and slowly faded to 93 mAh g^{-1} after 200 cycles, accompanied by a stable coulombic efficiency of 98%. The slightly lower efficiency indicated that there were minor side reactions between the electrode and electrolyte, and it also led to the increase of charge transfer resistance (R_{ct}) along with the cycle number (Figure S8 and Table S1). This might be the main reason of capacity decay because both anode and cathode were insoluble in the electrolyte. In Figure 3C, we tried to predict the full-cell charge/discharge curve by subtracting the voltage profile of the anode from that of the cathode and then found that the experimental curve completely coincided with the calculated one. The charge/discharge curve had two plateaus with equal specific capacity and small charge/discharge voltage gap of 0.11 V (Figure S9), indicating the low polarization and highly reversible character of PI5/EMITFSI/PTPAn full-cell. In Figures 3D and 3E, strikingly excellent rate performance was exhibited. Even up to 200 C, 70% of the 1 C capacity could be reserved (the charge or discharge process could be completed in 12.6 s). In addition, the capacity could fully recover with the current returning to 1 C. Increasing coulombic efficiency was observed at higher current rate, mostly above 99% during the test. Obvious polarization increment was only observed at very high current rate of above 100 C (Figure 3E). Furthermore, considering the possible practical application, the relatively higher loading electrode (Table S2) was also tested. In Figure S10, an as-good rate performance up to 40 C could be observed. Long-term cycling was tested at 20 C (Figure 3F). After 5,000 cycles, the specific capacity was maintained above 80 mAh g^{-1}, about 75% of its maximum value (107 mAh g^{-1}), accompanied by a 100% coulombic efficiency. Now it could be concluded that owing to pure ionic liquid electrolyte the PI5/EMITFSI/PTPAn metal-free battery had achieved breakthrough improvement in electrochemical performance.

The redox mechanism of the full-cell was investigated by XPS by tracing the evolvement of energy bands of some characteristic groups (Figure 4). For PI5 anode, the energy band of –C=O group at 289.4 eV could be observed in the fresh electrode and discharged electrode, whereas PI5 being charged in the full-cell, another energy band of –C–O$^-$ bond at 287.1 eV appeared instead, indicating the reversible reduction/oxidation of carbonyl group. For PTPAn cathode, reversible transformation between tertiary amine and tertiary ammonium cation could be monitored by the appearance/disappearance of the energy band at 402.5 eV (–C$_3$N$^+$). Thus the XPS analysis verified that ion-doping reaction reversibly happened in PI5 and PTPAn as reported previously (Gador et al., 1998; Qiu et al., 2015) even in pure and metal-ion-absent ionic liquid (Figure 1C).

The low-temperature property was always a bottleneck as regards the application of ionic liquid, hence we evaluated the PI5/EMITFSI/PTPAn full-cell again under different temperatures. For conventional Li-ion batteries, the reaction kinetics at low temperature was more affected by the slow solid ion diffusion and/or
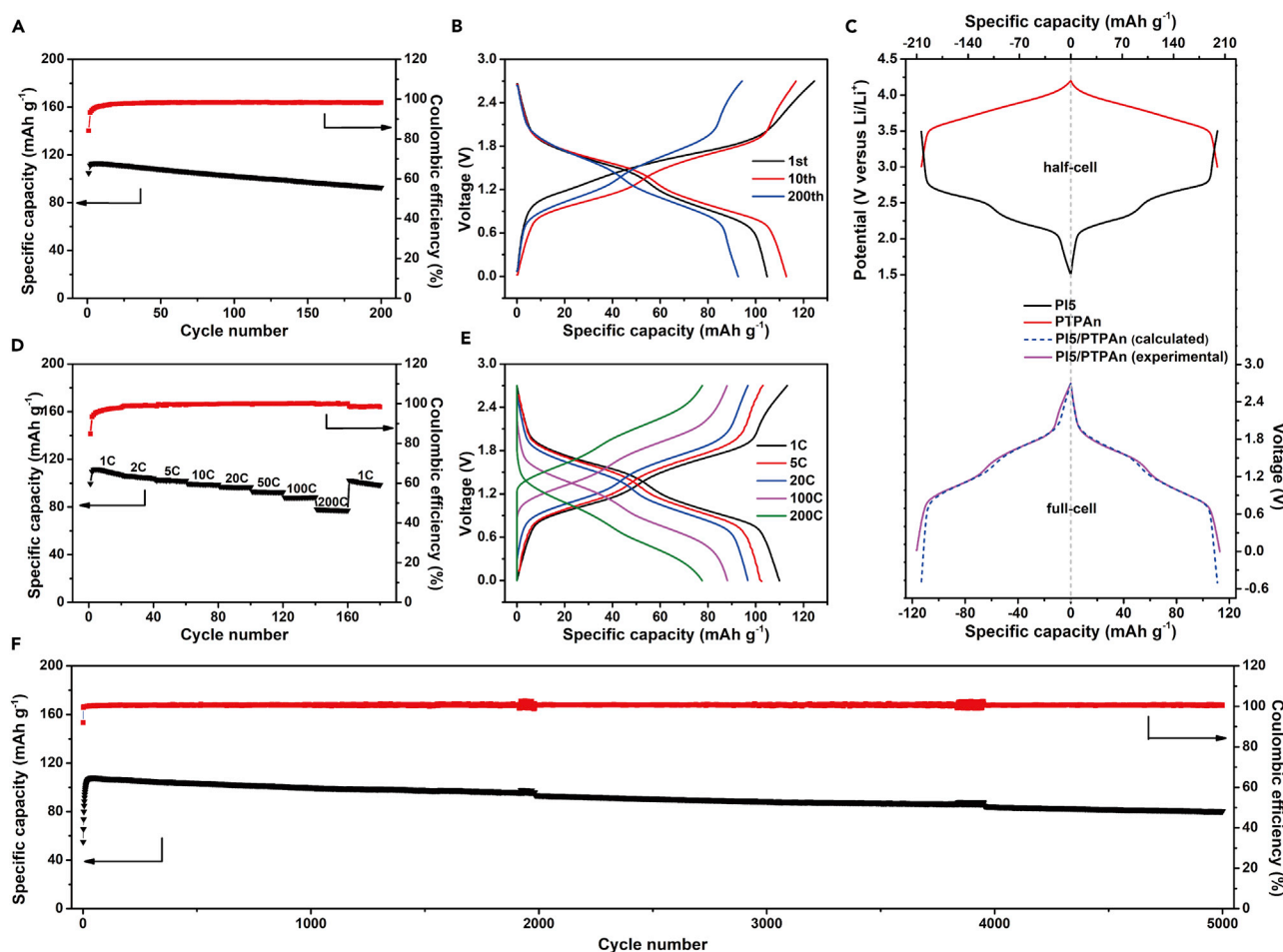
Figure 3. Electrochemical Performance of PI5/PTPAn Full-Cell with Pure EMITFSI

(A and B) (A) The cycling performance and (B) corresponding voltage profiles at 1 C rate.

(C) Comparison of the experimental and the calculated voltage profiles of PI5/PTPAn full cell (the calculated curve was obtained by subtracting the charging/discharging curve of PI5 anode from that of PTPAn cathode).

(D and E) (D) The rate performance and (E) corresponding voltage profiles; the rate was stepwise changed from 1 C to 200 C.

(F) The long-term cycling performance at 20 C within 5,000 cycles.

high SEI resistance, and poor capacity retention was thus usually observed (Luo et al., 2014; Plichta et al., 2001). On the contrary, for our metal-free battery, the pseudocapacitive reaction nature of PI5 and PTPAn as well as the still-high ionic conductivity of EMITFSI at −10°C (Figure S7) implied that the low-temperature performance of PI5/PTPAn cell could be expected. In Figure 5A, the discharge capacity and coulombic efficiency of the full-cell was plotted against cycle number at 30°C, 10°C, and −10°C (lower-temperature test was not conducted because the freezing point of EMITFSI was −12°C, Garcia et al., 2004). At −10°C, increased electrochemical impedance (Figure S11 and Table S1) brought lower discharge capacity in the initial cycle, but the capacity could reach 107 mAh g^{-1} after some "activation" cycles, after which superflat cycling curve could also be observed (99.8% capacity retention after 200 cycles). The results indicated that low temperature had two effects on the cell performance. On one hand, lower temperature caused higher viscosity and further incurred a longer activation process to get the electrode sufficiently infiltrated. On the other hand, low temperature greatly reduced the occurrence of side reactions and we thus saw improved cycling stability and coulombic efficiency at −10°C than 30°C. Low temperature led to very insignificant change in the charge/discharge curves (Figure 5B), suggesting that the high redox reversibility was well maintained at low temperature. Moreover, the fast reaction kinetics was also preserved at low temperature and the PI5/PTPAn full-cell presented decent rate capability under −10°C and delivered appreciable capacity of 79 mAh g^{-1} at 50 C (Figure 5C), accompanied by acceptable voltage polarization (Figure 5D).
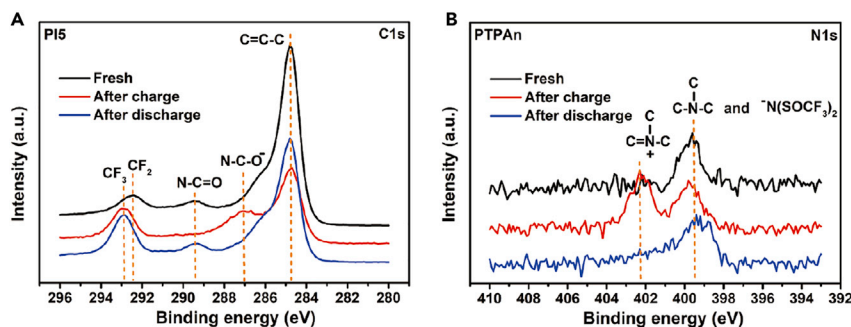
Figure 4. X-ray photo-electron spectroscopy (XPS) Analysis of PI5 Anode and PTPAn Cathode at Various Charge/Discharge States

(A and B) (A) C1s spectra of PI5 anode and (B) N1s spectra of PTPAn cathode in various states of fresh electrode, after the first charge and after the first discharge. Note that PI5 and PTPAn were removed from the PI5/EMITFSI/PTPAn full-cell after the first charge or discharge. The bands at 292.4 eV for $-CF_2$ and 292.9 eV for $-CF_3$ in (A) should be ascribed to PTFE binder and the residual $TFSI^-$, respectively. In (B), the energy band of $-C_3N$ at around 399.5 eV in charged PTPAn should be attributed to $TFSI^-$ (Zheng et al., 2013) doping accompanied by PTPAn oxidation.

Non-flammability of Pure Ionic Liquid Electrolyte

Ionic liquid had been known for its non-volatility, non-flammability, and thermal stability, and it was thus widely used as additive or co-solvent for safety enhancement of the aprotic electrolyte. In Figure 6, we compared the flammability of three kinds of electrolytes including conventional 1 M LiTFSI/EC + DEC electrolyte, pure EMITFSI, and their 1:1 (volume ratio) mixture, which was typically used in the report about non-flammable electrolyte (Guerfi et al., 2010). The combustion experiment was conducted following the protocol used in a previous study (Wu et al., 2015). A piece of glass fiber disk soaked with electrolyte was ignited, and pictures were taken after different time intervals to record the burning process. As anticipated, the conventional ester electrolyte burned immediately and kept burning for 22 s. The hybrid electrolyte was less flammable and extinguished after 16 s, with some black ashes left on the disk. Among them, the pure EMITFSI electrolyte was totally non-flammable during a test time of 25 s, suggesting the distinct safety advantage of the PI5/EMITFS/PTPAn cell.

Universality of Metal-free Battery Concept

Inspired by the above results, we thought the reversible interaction of organic cations other than EMI^+ could also happen on n-type organic anode, and thus many other ionic liquids might be applied in metal-free battery. To prove it, another two kinds of ionic liquids, pure BMPTFSI and ATEATFSI, were used as the electrolyte in the PI5/PTPAn full-cell. Despite the bigger ionic size of BMP^+ (0.339 nm) and $ATEA^+$, it exhibited similar capacity performance and cycling stability at 1 C rate to that in EMITFSI (Figure S12A), except the initial several ''activation'' cycles. The charge/discharge curves in BMPTFSI and ATEATFSI electrolytes were also quite similar to that in EMITFSI, with slightly increased voltage polarization (Figure S12B). The results could be explained by the higher viscosity and lower ionic conductivity of BMPTFSI and ATEATFSI than EMITFSI (Figure S13), which caused increased electrolyte resistance (R_s) and charge transfer resistance (R_{ct}) in electrochemical impedance spectroscopy (EIS) tests (Figure S14 and Table S1). In spite of the slower reaction kinetics, the successful application of BMPTFSI and ATEATFSI suggested the wide range of electrolyte options when building the metal-free battery.

Not merely the electrolyte, the n-type anode was also not necessarily limited to PI5. In view of the lower redox potential of anode being preferred for the full-cell, PI2 and PAQ anodes were studied. Unfortunately, they turned out to be unsuitable anodes in EMITFSI, probably due to some compatibility issues with the electrolyte. The results in Figure S15 indicated that PI2 and PAQ both had better utilization and cycling stability in ether electrolyte of 1 M LiTFSI/DOL + DME. Although in pure EMITFSI, the performances of PI2 and PAQ were far from expectation, they either showed poorer capacity retention (47% after 50 cycles for PI2) or lower capacity (95 mAh g^{-1} for PAQ). The compatibility issues might be generated by the poor wettability of the electrode, the side reactions, and even the altered reaction kinetics, which needed to be further investigated. We also evaluated the performance of the full-cell with PI or PAQ anode. In Figure S16, the lower capacity of PAQ accordingly decreased the capacity release of PAQ/PTPAn full-cell, whereas the worse capacity retention of PI2 deteriorated the cycling stability of PI2/PTPAn full-cell. However, the
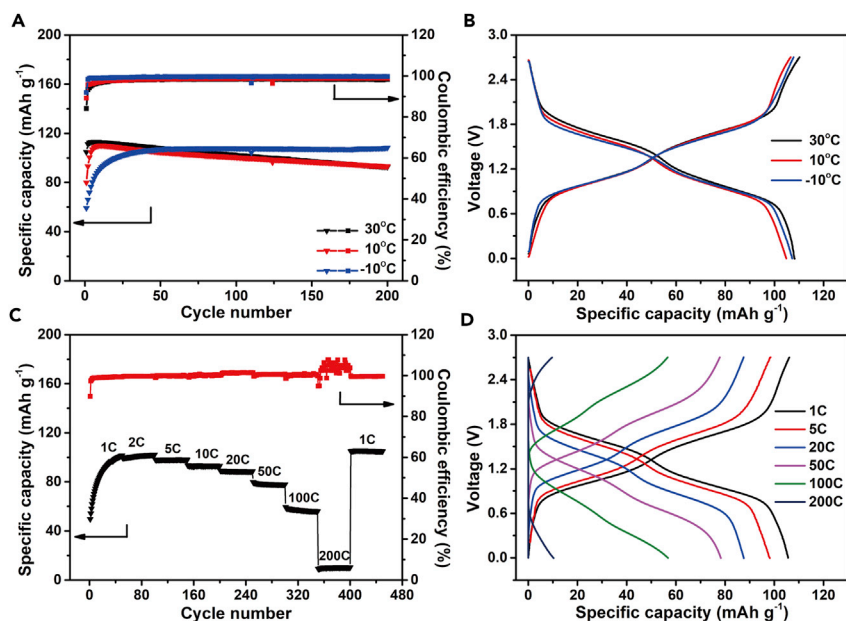
Figure 5. Low-Temperature Performance of PI5/PTPAn Full-Cell with Pure EMITFSI Electrolyte
(A and B) The (A) cycling performance and (B) voltage profiles (from the 50th cycle) under 1 C rate at temperatures of 30°C, 10°C, and −10°C.
(C and D) The (C) rate performance and (D) voltage profiles at −10°C under stepwise increasing current rate from 1 C to 200 C.

remarkably elevated discharge voltage (1.67 V) of PI2/PTPAn full-cell still should be mentioned, because it implied that for the foreseeable future, the energy density of the metal-free battery was very likely improved by using the n-type organic anode with much lower redox potential and good compatibility with ionic liquid. For instance, di-lithium terephthalate showed so far the lowest redox potential of 1.0 V versus Li$^+$/Li in the organic electrode family (Armand et al., 2009b).

DISCUSSION

In conclusion, highly reversible intercalation/deintercalation reaction of organic cation with n-type organic electrode was first revealed. The metal-free battery was thus constructed by connecting n-type organic anode and p-type organic cathode using pure ionic liquid electrolyte. The PI5/EMITFSI/PTPAn full battery demonstrated good specific capacity release, strikingly high rate performance of 70% capacity reserved at 200 C, outstanding long-term cycling stability of 75% capacity retention after 5,000 cycles, and remarkable low-temperature performance. The pseudocapacitive electrochemical redox of PI5 and PTPAn in EMITFSI was facilitated by the high ionic conductivity, highly available unpaired cation/anion, and non-solvation character of pure ionic liquid electrolyte. In addition, the novel, metal-free battery was intrinsically non-flammable, resource-sustainable, environment friendly, and potentially recyclable. Our pioneer work revealed alternative strategy for future energy storage. First, the energy density still has huge margin of improvement because of the wide electrochemical window of ionic liquid (up to 6 V) (Eftekhari et al., 2016), the structural diversity of organic electrode materials, and thus tunable cell voltage and capacity, Second, wide-temperature-range battery can be readily fulfilled by adjusting the electrolyte recipe as required, and the ionic liquid with lower freezing point and higher stability/compatibility with organic electrode will being perused. Third, the flexibility of polymer electrode and inherent safety of ionic liquid endow it with potential application in flexible and wearable batteries. Therefore the metal-free battery is not only a conceptional innovation but also a competitive candidate in future sustainable and versatile energy storage applications, whether small electronic components, electric vehicle batteries, or even grid energy storage.

Limitations of the Study

Here, we provided a novel metal-free and solvent-free battery conception and realized it by n-type organics/ionic liquid/p-type organics full-cell. In the above, the fast reaction kinetics, ultra-long cycling
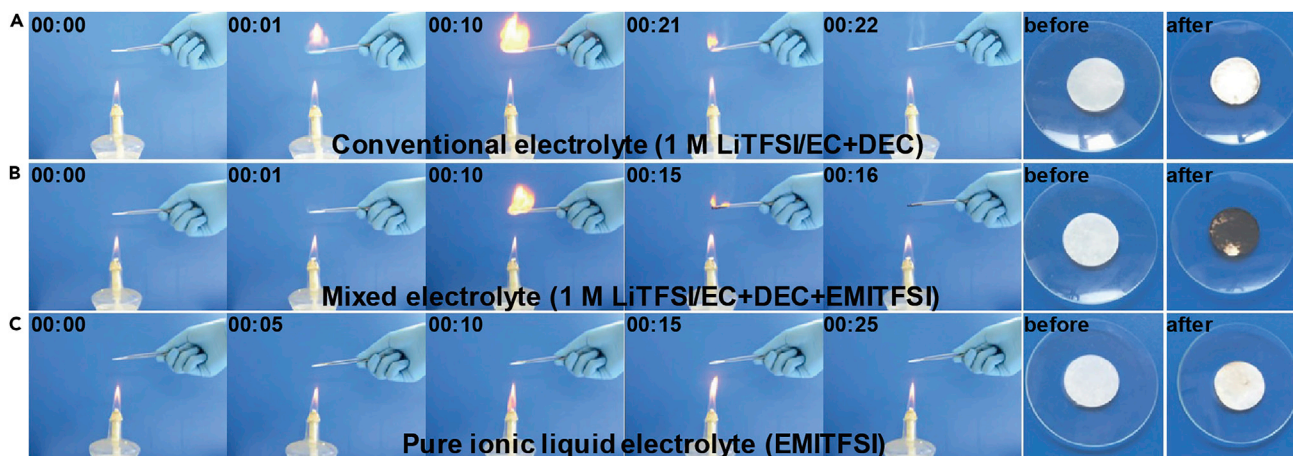
Figure 6. Flammability Test of the Three Types of Electrolytes
(A–C) A piece of glass fiber disk was wetted by 0.3 mL (A) conventional 1 M LiTFSI/EC + DEC (1:1, v/v), (B) hybrid electrolyte of 1 M LiTFSI/EC + DEC + EMITFSI (1:1:2, v/v/v), and (C) pure EMITFSI, and then ignited by an alcohol burner. The combustion phenomena were recorded by a camera, and typical pictures at different times (in second) after igniting were presented to show the combustion process. The images in the rightmost two rows showed the glass fiber disk before and after burning.

stability, and as-good low-temperature performance of PI5/EMITFSI/PTPAn cell was fully displayed. However, we also noticed that the attempt to use other organics such as PI2 and PAQ to construct the metal-free battery was not very successful. The fact implied the incompatibility between the electrode material and electrolyte and suggested that the metal-free battery was much more profound than currently discussed. Further in-depth investigation is needed to fully understand the brand new battery and make the battery concept and construction really universal. In addition, it has to be pointed out that the cost is always a primary concern in the commercial application of any novel battery, and hence the current high price of ionic liquid may be the biggest issue. However, the price is tightly related to the market. For example, owing to the expansion of Li-ion battery market and technical progress, the price of commercial electrolyte of $LiPF_6$ in EC + dimethyl carbonate (DMC) decreased by dozens of times from the late 1990s to now. Moreover, compared with $LiPF_6$ or other lithium salt, the much less reactivity toward water of ionic liquids may lead to easier production and storage, and in turn can greatly alleviate the cost issue.

METHODS

All methods can be found in the accompanying Transparent Methods supplemental file.

SUPPLEMENTAL INFORMATION

Supplemental Information can be found online at https://doi.org/10.1016/j.isci.2019.04.010.

ACKNOWLEDGMENTS

AUTHOR CONTRIBUTIONS

J.Q., Z.S., and H.Z. conceived the idea and co-wrote the manuscript. J.Q. carried out the experiments. F.M. offered many useful suggestions throughout the experiment. N.L. helped with part of material preparation and physical characterization. Q.L. helped with part of flammability test and ionic conductivity test. X.W. helped with high loading electrode test (Figure S10 data).

DECLARATION OF INTERESTS

The authors declare no competing interests.

REFERENCES

Armand, M., Endres, F., MacFarlane, D.R., Ohno, H., and Scrosati, B. (2009a). Ionic-liquid materials for the electrochemical challenges of the future. Nat. Mater. 8, 621–629.

Armand, M., Grugeon, S., Vezin, H., Laruelle, S., Ribière, P., Poizot, P., and Tarascon, J.M. (2009b). Conjugated dicarboxylate anodes for Li-ion batteries. Nat. Mater. 8, 120–125.

Augustyn, V., Come, J., Lowe, M.A., Kim, J.W., Taberna, P.L., Tolbert, S.H., Abruna, H.D., Simon, P., and Dunn, B. (2013). High-rate electrochemical energy storage through Li^+ intercalation pseudocapacitance. Nat. Mater. 12, 518–522.

Bitenc, J., Pirnat, K., Bančič, T., Gaberšček, M., Genorio, B., Randon-Vitanova, A., and Dominko, R. (2015). Anthraquinone-based polymer as cathode in rechargeable magnesium batteries. ChemSusChem 8, 4128–4132.

Bruce, P.G., Freunberger, S.A., Hardwick, L.J., and Tarascon, J.M. (2012). Li–O_2 and Li–S batteries with high energy storage. Nat. Mater. 11, 19–29.

Deng, W., Liang, X., Wu, X., Qian, J., Cao, Y., Ai, X., Feng, J., and Yang, H. (2013). A low cost, all-organic Na-ion battery based on polymeric cathode and anode. Sci. Rep. 3, 2671.

Dong, X., Guo, Z., Guo, Z., Wang, Y., and Xia, Y. (2018). Organic batteries operated at −70°C. Joule 2, 902–913.

Eftekhari, A., Liu, Y., and Chen, P. (2016). Different roles of ionic liquids in lithium batteries. J. Power Sources 334, 221–239.

Fan, J., Zhang, Z., Liu, Y., Wang, A., Li, L., and Yuan, W. (2017). An excellent rechargeable PP_{14} TFSI ionic liquid dual-ion battery. Chem. Commun. (Camb.) 53, 6891–6894.

Feng, J.K., Cao, Y.L., Ai, X.P., and Yang, H.X. (2008). Polytriphenylamine: a high power and high capacity cathode material for rechargeable lithium batteries. J. Power Sources 177, 199–204.

Fu, Y., Chen, C., Qiu, C., and Ma, X. (2009). Vinyl ethylene carbonate as an additive to ionic liquid electrolyte for lithium ion batteries. J. Appl. Electrochem. 39, 2597–2603.

Gador, D., Buchberger, C., Fink, R., and Umbach, E. (1998). "Manipulation" of molecular orientation in ultrathin organic films: NTCDA on Ag (111). EPL (Europhy. Lett.) 41, 231.

Garcia, B., Lavallée, S., Perron, G., Michot, C., and Armand, M. (2004). Room temperature molten salts as lithium battery electrolyte. Electrochim. Acta 49, 4583–4588.

Gloe, K., Stephan, H., and Grotjahn, M. (2003). Where is the anion extraction going? Chem. Eng. Technol. 26, 1107–1117.

Guerfi, A., Dontigny, M., Charest, P., Petitclerc, M., Lagacé, M., Vijh, A., and Zaghib, K. (2010). Improved electrolytes for Li-ion batteries: mixtures of ionic liquid and organic electrolyte with enhanced safety and electrochemical performance. J. Power Sources 195, 845–852.

Hao, F., Lin, H., Liu, Y., and Li, J. (2011). Anionic structure-dependent photoelectrochemical responses of dye-sensitized solar cells based on a binary ionic liquid electrolyte. Phys. Chem. Chem. Phys. 13, 6416–6422.

Hong, W., Meis, C., Heflin, J.R., and Montazami, R. (2014). Evidence of counterion migration in ionic polymer actuators via investigation of electromechanical performance. Sensor. Actuat. B Chem. 205, 371–376.

Hu, J.J., Long, G.K., Liu, S., Li, G.R., and Gao, X.P. (2014). A LiFSI–LiTFSI binary-salt electrolyte to achieve high capacity and cycle stability for a Li–S battery. Chem. Commun. (Camb.) 50, 14647–14650.

Jian, Z., Liang, Y., Rodríguez-Pérez, I.A., Yao, Y., and Ji, X. (2016). Poly (anthraquinonyl sulfide) cathode for potassium-ion batteries. Electrochem. Commun. 71, 5–8.

Jung, S.K., Kim, H., Cho, M.G., Cho, S.P., Lee, B., Kim, H., Park, Y.U., Hong, J., Park, K.Y., Seong, W.M., et al. (2017). Lithium-free transition metal monoxides for positive electrodes in lithium-ion batteries. Nat. Energy 2, 16208.

Larcher, D., and Tarascon, J.M. (2015). Towards greener and more sustainable batteries for electrical energy storage. Nat. Chem. 7, 19–29.

Levin, E.E., Vassiliev, S.Y., and Nikitina, V.A. (2017). Solvent effect on the kinetics of lithium ion intercalation into $LiCoO_2$. Electrochim. Acta 228, 114–124.

Liang, Y., and Yao, Y. (2018). Positioning organic electrode materials in the battery landscape. Joule 2, 1690–1706.

Liang, Y., Tao, Z., and Chen, J. (2012). Organic electrode materials for rechargeable lithium batteries. Adv. Energy Mater. 2, 742–769.

Lu, J., Yang, J.X., Wang, J., Lim, A., Wang, S., and Loh, K.P. (2009). One-pot synthesis of fluorescent carbon nanoribbons, nanoparticles, and graphene by the exfoliation of graphite in ionic liquids. ACS Nano 3, 2367–2375.

Luo, Y., Xu, X., Zhang, Y., Pi, Y., Zhao, Y., Tian, X., An, Q., Wei, Q., and Mai, L. (2014). Hierarchical carbon decorated $Li_3V_2(PO_4)_3$ as a bicontinuous cathode with high-Rate capability and broad temperature adaptability. Adv. Energy Mater. 4, 1400107.

MacFarlane, D.R., Forsyth, M., Howlett, P.C., Kar, M., Passerini, S., Pringle, J.M., Ohno, H., Watanabe, M., Yan, F., Zhang, S., et al. (2016). Ionic liquids and their solid-state analogues as materials for energy generation and storage. Nat. Rev. Mater. 1, 15005.

Muldoon, J., Bucur, C.B., and Gregory, T. (2014). Quest for nonaqueous multivalent secondary batteries: magnesium and beyond. Chem. Rev. 114, 11683–11720.

Nitta, N., Wu, F., Lee, J.T., and Yushin, G. (2015). Li-ion battery materials: present and future. Mater. Today 18, 252–264.

Van Noorden, R. (2014). The rechargeable revolution: a better battery. Nature 507, 26–28.

Piper, D.M., Evans, T., Leung, K., Watkins, T., Olson, J., Kim, S.C., Han, S.S., Bhat, V., Oh, K.H., Lee, S.H., et al. (2015). Stable silicon-ionic liquid interface for next-generation lithium-ion batteries. Nat. Commun. 6, 6230.

Plichta, E.J., Hendrickson, M., Thompson, R., Au, G., Behl, W.K., Smart, M.C., Ratnakumar, B.V., and Surampudi, S. (2001). Development of low temperature Li-ion electrolytes for NASA and DoD applications. J. Power Sources 94, 160–162.

Qin, H., Song, Z.P., Zhan, H., and Zhou, Y.H. (2014). Aqueous rechargeable alkali-ion batteries with polyimide anode. J. Power Sources 249, 367–372.

Qiu, B., Xu, C., Sun, D., Wang, Q., Gu, H., Zhang, X., Weeks, B.L., Hopper, J., Ho, T.C., Wei, S., et al. (2015). Polyaniline coating with various substrates for hexavalent chromium removal. Appl. Surf. Sci. 334, 7–14.

Read, J.A., Cresce, A.V., Ervin, M.H., and Xu, K. (2014). Dual-graphite chemistry enabled by a high voltage electrolyte. Energy Environ. Sci. 7, 617–620.

Rui, X., Sun, W., Wu, C., Yu, Y., and Yan, Q. (2015). An advanced sodium-ion battery composed of carbon coated $Na_3V_2(PO_4)_3$ in a porous graphene network. Adv. Mater. 27, 6670–6676.

Schon, T.B., McAllister, B.T., Li, P.F., and Seferos, D.S. (2016). The rise of organic electrode materials for energy storage. Chem. Soc. Rev. 45, 6345–6404.

Slater, M.D., Kim, D., Lee, E., and Johnson, C.S. (2013). Sodium-ion batteries. Adv. Funct. Mater. 23, 947–958.

Song, Z., and Zhou, H. (2013). Towards sustainable and versatile energy storage

devices: an overview of organic electrode materials. Energy Environ. Sci. 6, 2280–2301.

Song, Z., Zhan, H., and Zhou, Y. (2009). Anthraquinone based polymer as high performance cathode material for rechargeable lithium batteries. Chem. Commun. (Camb.) 4, 448–450.

Song, Z., Zhan, H., and Zhou, Y. (2010). Polyimides: promising energy-storage materials. Angew. Chem. Int. Ed. 122, 8622–8626.

Tokuda, H., Hayamizu, K., Ishii, K., Susan, M.A.B.H., and Watanabe, M. (2004). Physicochemical properties and structures of room temperature ionic liquids. 1. Variation of

anionic species. J. Phys. Chem. B 108, 16593–16600.

Wang, L., Liu, J., Yuan, S., Wang, Y., and Xia, Y. (2016). To mitigate self-discharge of lithium–sulfur batteries by optimizing ionic liquid electrolytes. Energy Environ. Sci. 9, 224–231.

Wu, F., Zhu, Q., Chen, R., Chen, N., Chen, Y., and Li, L. (2015). Ring-chain synergy in ionic liquid electrolytes for lithium batteries. Chem. Sci. 6, 7274–7283.

Yabuuchi, N., Kubota, K., Dahbi, M., and Komaba, S. (2014). Research development on

sodium-ion batteries. Chem. Rev. 114, 11636–11682.

Zhang, Y., Huang, Y., Yang, G., Bu, F., Li, K., Shakir, I., and Xu, Y. (2017). Dispersion–assembly approach to synthesize three-dimensional graphene/polymer composite aerogel as a powerful organic cathode for rechargeable Li and Na batteries. ACS Appl. Mater. Interfaces 9, 15549–15556.

Zheng, J., Gu, M., Chen, H., Meduri, P., Engelhard, M.H., Zhang, J.G., Liu, J., and Xiao, J. (2013). Ionic liquid-enhanced solid state electrolyte interface (SEI) for lithium–sulfur batteries. J. Mater. Chem. A 1, 8464–8470.

Supplemental Information

A Metal-free Battery

with Pure Ionic Liquid Electrolyte

Jian Qin, Qing Lan, Ning Liu, Fang Men, Xin Wang, Zhiping Song, and Hui Zhan
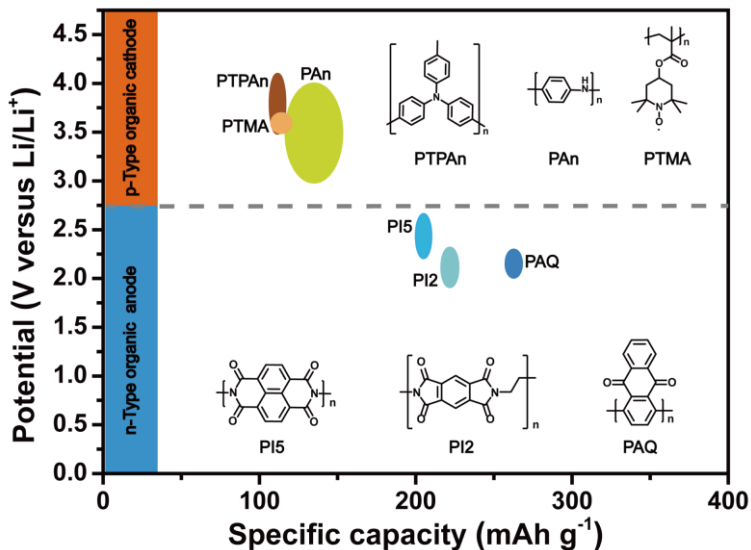
Figure S1. Schematic diagram of p-Type and n-Type electrode materials, related to Figure 1. The voltage, capacity, and structure of p-type organic cathode candidates and n-type organic anode candidates for metal-free batteries: polytriphenylamine (PTPAn), polyaniline (PAn), poly(2,2,6,6-tetramethylpiperidine-1-oxyl-4-yl methacrylate) (PTMA), polyimide (PI2 and PI5), and polyanthraquinone (PAQ) (Song et al., 2013).
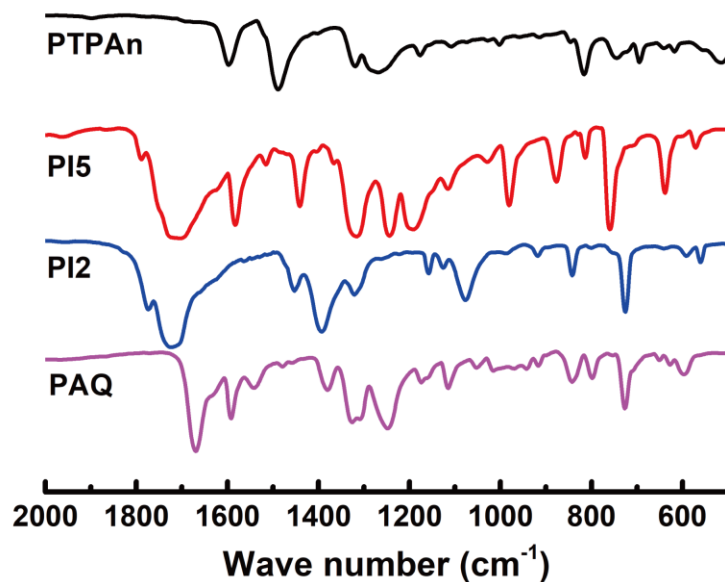
Figure S2. Characterization of electrode active materials, related to Figure 3.
FTIR spectra (KBr pellets) of the polymers involved in this paper, including PTPAn, PI5, PI2, and PAQ. All the characteristic peaks were consistent with the literature values: for PTPAn (Deng et al., 2013), 1597, 1489, 1319, 1269, 816 cm^{-1}; for PI5 (Song et al., 2010), 1705, 1583, 1317, 1117, 760 cm^{-1}; for PI2 (Song et al., 2010), 1774, 1724, 1392, 726 cm^{-1}; for PAQ (Song et al., 2009), 1670, 1591, 1541, 1379, 1326, 1309, 1248, 1174, 1115, 843, 798, 727, 596 cm^{-1}.
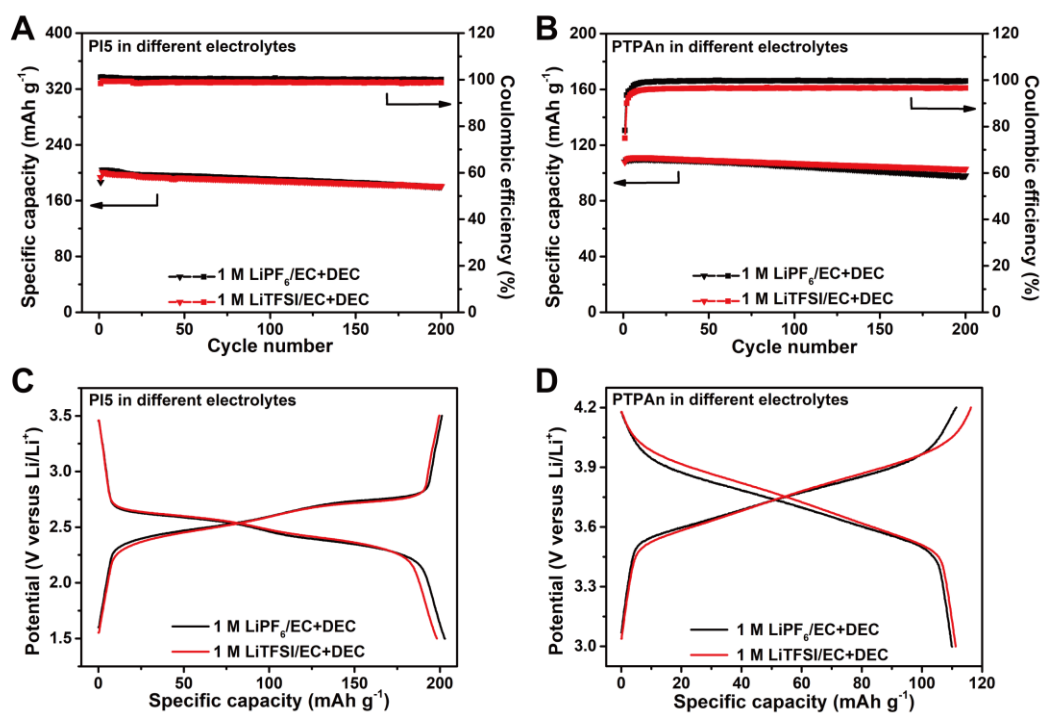
Figure S3. Results of Half-cell tests of PI5 and PTPAn, related to Figure 2.

The cycling performance (A, B) and typical voltage profiles (C, D) (from the 10th cycle) of PI5 and PTPAn half-cell with conventional ester electrolytes containing different salts (1 M $LiPF_6$ or LiTFSI in EC+DEC) at 1 C rate. Compared to $TFSI^-$, PF_6^- could obviously improve the stable Coulombic efficiency of PTPAn from 96.6% to 99.6%, probably due to its higher oxidative stability than $TFSI^-$ at high charging potential. However, PF_6^- was not suitable to compose a pure ion liquid electrolyte due to the high melting point or low ionic conductivity at room temperature (Hao et al., 2011).
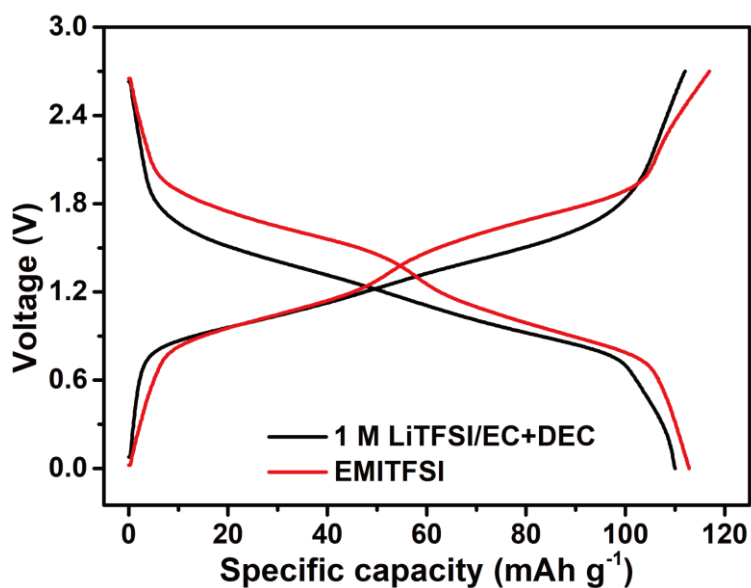
Figure S4. Comparison of PI5/PTPAn full-cells in different electrolytes, related to Figure 2.
Comparison of the typical voltage profiles (from the 10th cycle) of full-cell with conventional ester electrolyte of 1 M LiTFSI/EC+DEC and novel pure ion liquid electrolyte of EMITFSI at 1 C. The average discharge voltage of the latter (1.31 V) was obviously higher than that of the former (1.17 V), highly agreeing with the corresponding PI5 and PTPAn half-cell voltage profiles shown in Figure 2C and 2D.
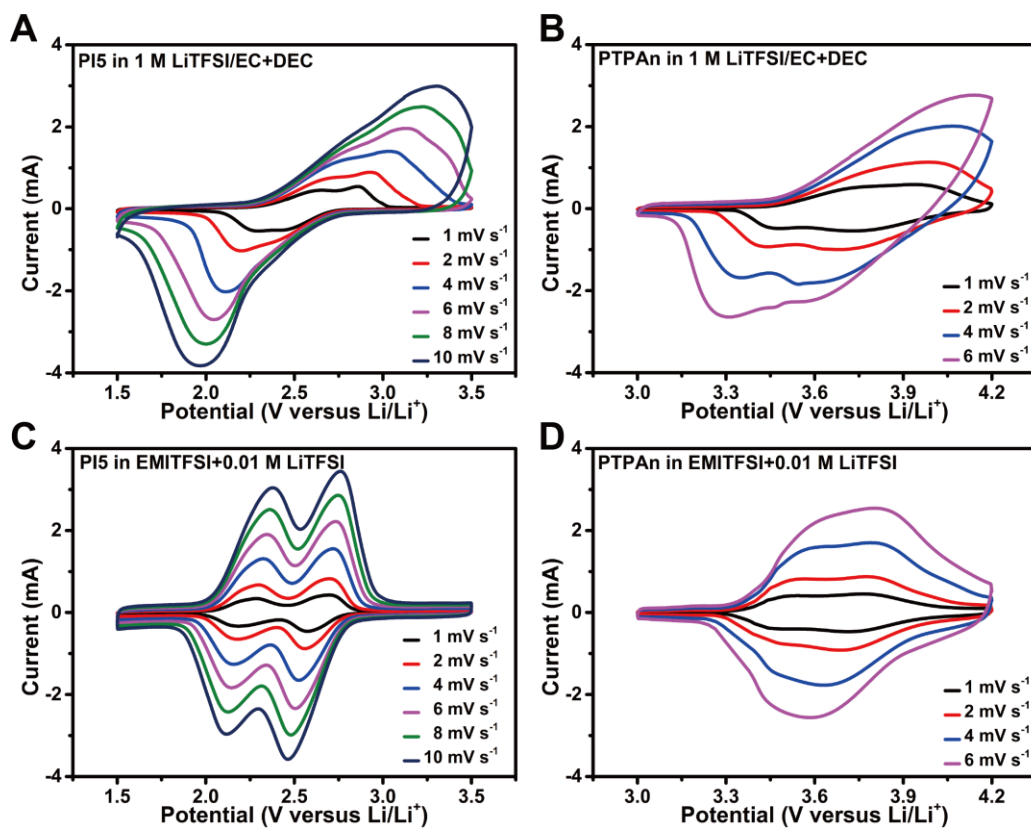
Figure S5. Reaction kinetic study of PI5 and PTPAn, related to Figure 2.
Comparison of the typical CV curves of PI5 and PTPAn electrode in ester electrolyte (A, B) and ionic liquid electrolyte (C, D) at different scan rates from 1 mV s^{-1} to 10 mV s^{-1} (PI5) or 6 mV s^{-1} (PTPAn).
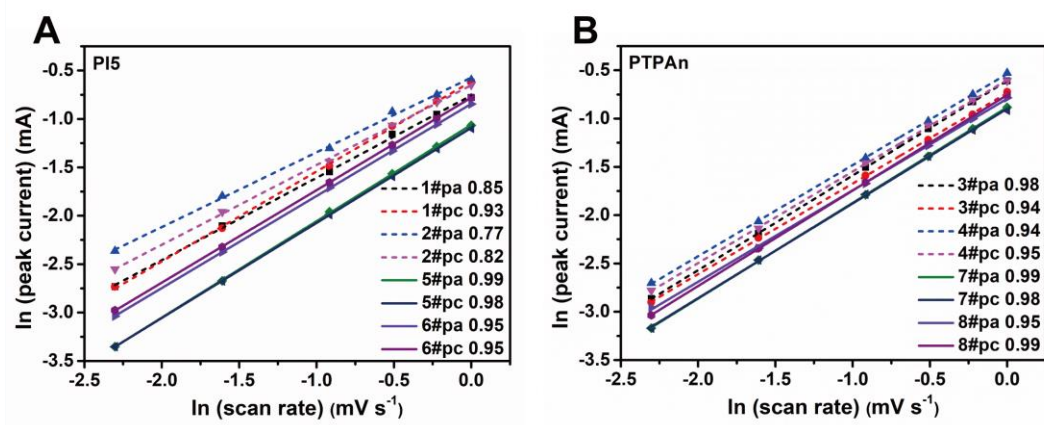
Figure S6. Reaction kinetic analysis of PI5 and PTPAn, related to Figure 2.
Anodic and cathodic peak current dependence on the scan rate derived from CV curves of PI5 (A) and PTPAn (B) in Figure 2G-2J. The data represented the slope of each fitted line which could explain the intercalation and capacitance contribution to the charge/discharge capacity (slope of 0.5 indicated complete intercalation reaction, while slope of 1 indicated complete capacitance reaction) in the two electrolytes of 1 M LiTFSI/EC+DEC (dash line) and EMITFSI+0.01 M LiTFSI (solid line). (pa: anodic peak, pc: cathodic peak)
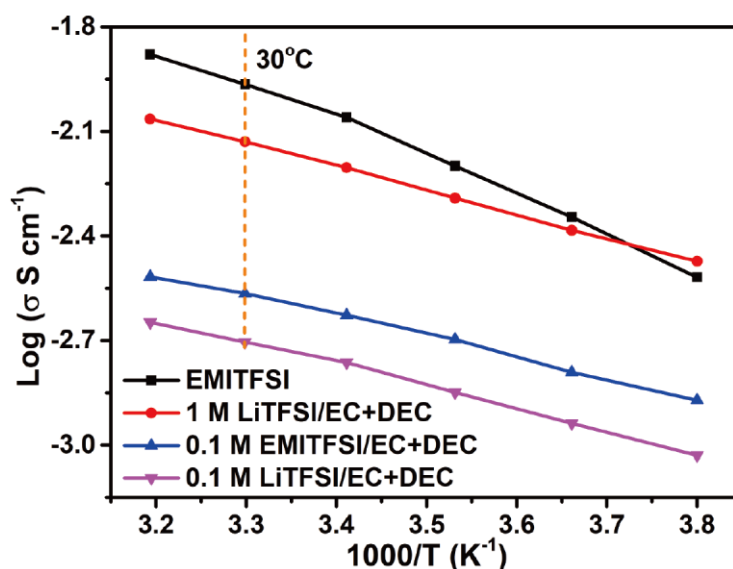
Figure S7. Ion conductivity study of different electrolytes, related to Figure 2.
Ionic conductivity profiles of different electrolytes (EMITFSI, 1 M LiTFSI/EC+DEC, 0.1 M EMITFSI/EC+DEC, and 0.1 M LiTFSI/EC+DEC) measured at temperature from 40°C to –10°C. In general, the ion-conductivity is determined by two factors, available ion and the speed of ion movement. Furthermore, the latter is mainly determined by the ion radius and solvent environment. Usually, in solvent-added electrolyte, the bigger ionic radius led to weakened coordination between the ion and solvent, and further weaker solvation and smaller solvated ion radius, which in turn greatly influenced the ion movement. The relationship above can be quantificationally depicted as $\sigma=nq^2D/KT$ (σ: *ionic* conductivity; n: ionic concentration; q: ionic electrical charge;: diffusion constant; K: Boltzmann's constant; T: absolute temperature), in which D is indicative of ion movement. The higher conductivity of EMITFSI than 1M LiTFSI/EC+DEC was attributed to its higher ionic concentration and possibly faster ion movement as well. On the other hand, when comparing diluent electrolytes of 0.1 M EMITFSI/EC+DEC and 0.1 M LiTFSI/EC+DEC, the effect of ion concentration and viscosity of ionic liquid could be substantially excluded. Hence, the determining factor in the above equation turned to the diffusion constant and the mirror relationship between D and σ could be established. In another word, σ is a reflection of D and vice versa. Given the same solvent environment, D value is mostly determined by the ion radius and further the conductivity order in turn becomes the supporting proof of the ion radius. Thus, in the comparison of 0.1 M EMITFSI/EC+DEC and 0.1 M LiTFSI/EC+DEC, the ions size order could be deduced from the conductivity order. Despite the bigger ion radius of EMI+ (0.294 nm) than Li+ (0.076 nm), in EC+DEC solvent, the solvated Li+ is very probably the larger one, and consequently, still higher conductivity was obtained in 0.1M EMITFSI in EC+DEC electrolyte.
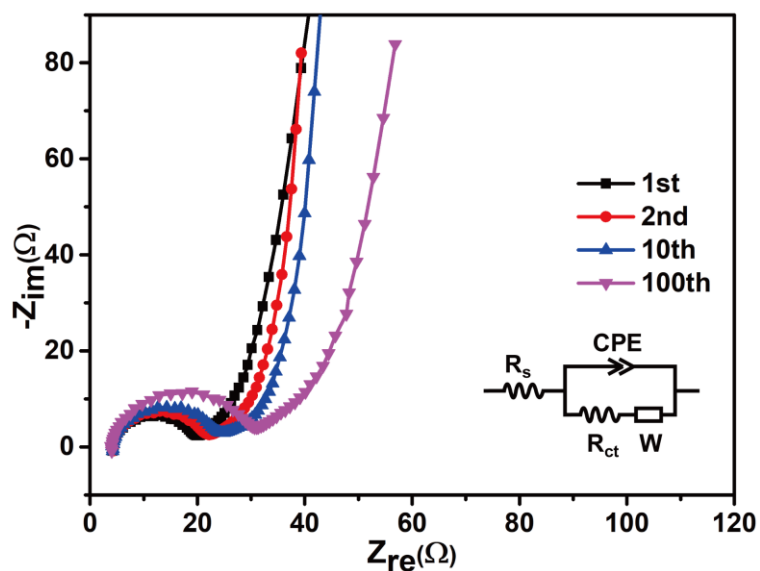
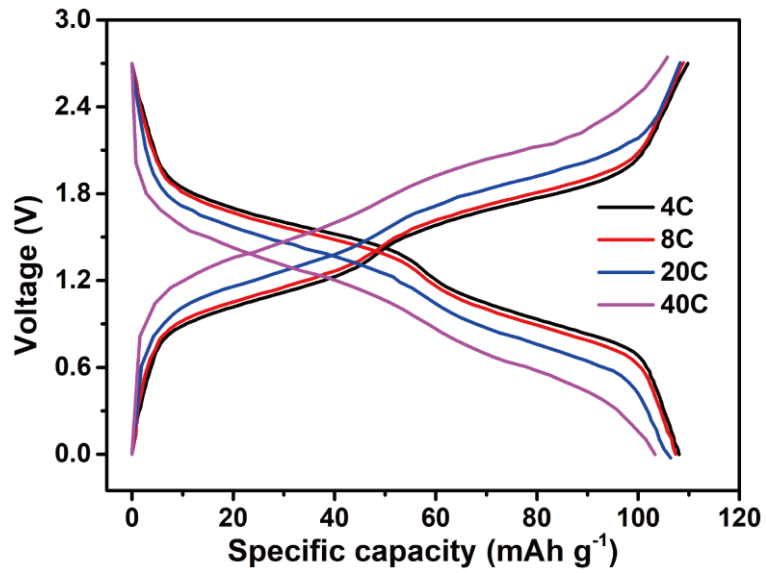**Figure S8. Impedance study of PI5/PTPAn full-cell, related to Figure 3.**

Nyquist plots of the PI5/PTPAn full-cell with EMITFSI electrolyte after 1st, 2nd, 10th, and 100th discharge process. The inset was the equivalent circuit used to fit the EIS data, where R_s, R_{ct}, CPE, and W represented solution resistance, charge transfer resistance, constant phase element, and Warburg impedance, respectively. The R_{ct} increased gradually from 13.8 Ω to 23.9 Ω during 100 cycles, indicating that the side reaction was not serious and the electrode status was relatively stable to sustain long-term cycling tests.
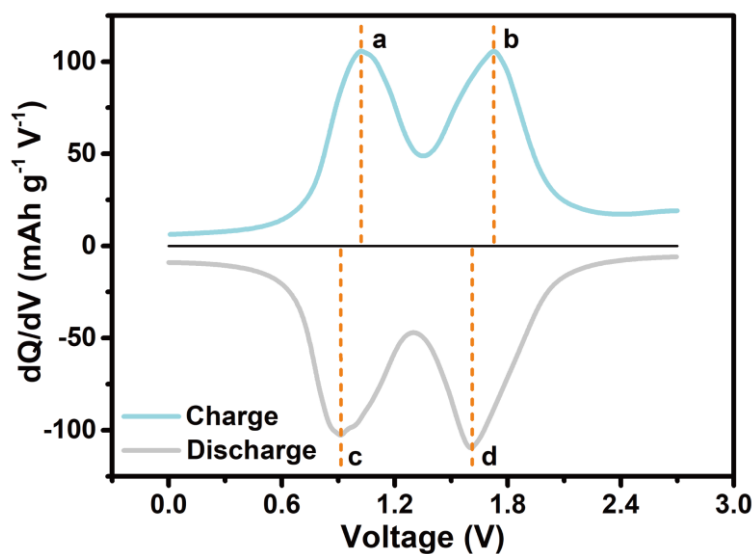
Figure S9. Charge/discharge plateau analysis of PI5/EMITFSI/PTPAn full-cell, related to Figure 3.

The differential (dQ/dV) curve calculated from the typical charge/discharge voltage profile of PI5/PTPAn full-cell with EMITFSI electrolyte (Figure 3B). The curve showed two pairs of symmetric redox peaks located at 1.02/0.91 V (a/c) and 1.72/1.61 V (b/d), respectively, with only a small gap of 0.11 V for both pairs. This was reasonable because either PI5 anode or PTPAn cathode undergone a highly reversible two-step redox process in the EMITFSI electrolyte (Fig. 2I and 2J).
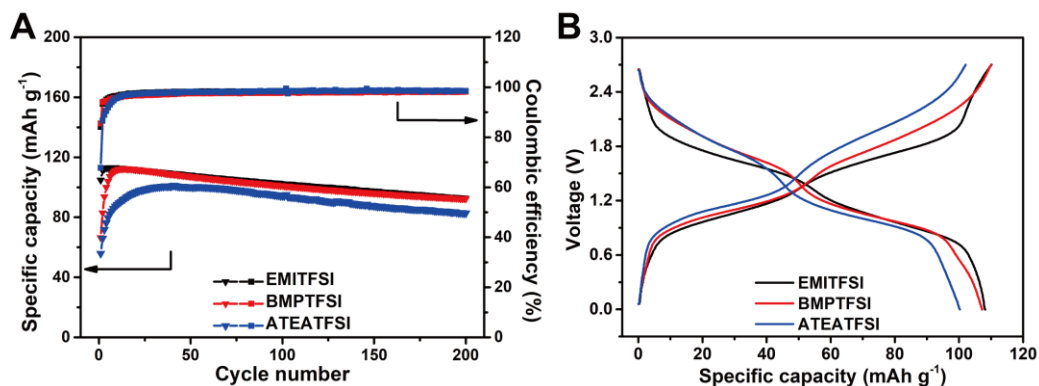
Figure S10. Electrochemical performance of PI5/EMITFSI/PTPAn full-cell, related to Figure 3.
The rate performance of PI5/EMITFSI/PTPAn full-cell using the high loading electrodes of PI5 and PTPAn (electrode information could be found in Table S2) with the current rate changed in step-wise mode from 4 C to 40 C.
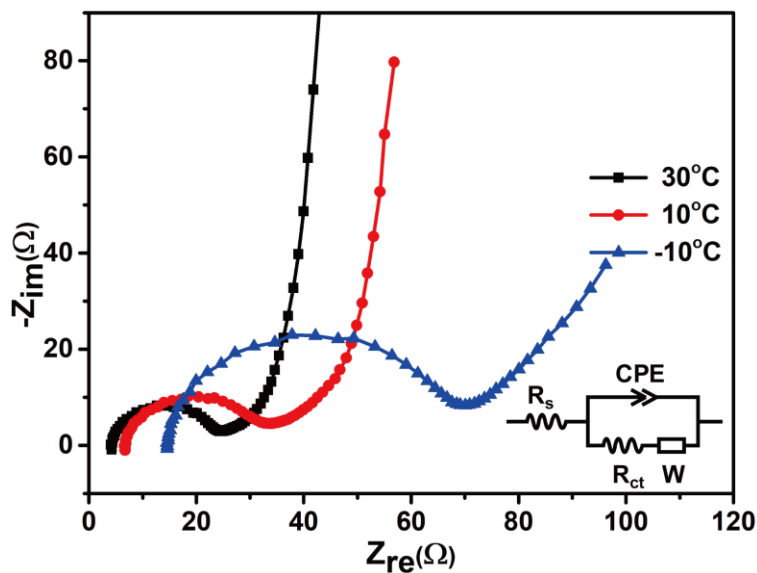
Figure S11. Impedance study of PI5/PTPAn full-cell at different temperature, related to Figure 5.

Nyquist plots of the PI5/PTPAn full-cell with EMITFSI electrolyte after the 10th discharge process at different temperatures and the corresponding equivalent circuit pattern. As the temperature was decreased from 30°C to 10°C and −10°C, the R_s grew from 4.09 Ω to 6.29 Ω and 14.2 Ω, while the R_{ct} grew from 18.9 Ω to 25.3 Ω and 47.7 Ω, indicating the lowering of electrolyte ionic conductivity and slowing of electrochemical reaction kinetics at lower temperature.

Figure S12. Electrochemical performance of PI5/PTPAn with different ionic liquid electrolytes, related to Figure 3.

The cycling performance (A) and typical voltage profiles (B, from the 50th cycle) of PI5/PTPAn full-cell with different pure ionic liquid electrolytes of EMITFSI, BMPTFSI, and ATEATFSI, respectively. Despite the appearance of initial cycles of "activation process" and the slight shape differences in voltage curves, the full-cell showed similar electrochemical behavior with BMPTFSI or ATEATFSI, as with EMITFSI electrolyte, indicating that the concept of metal-free battery was applicable for different pure ion liquid electrolytes.
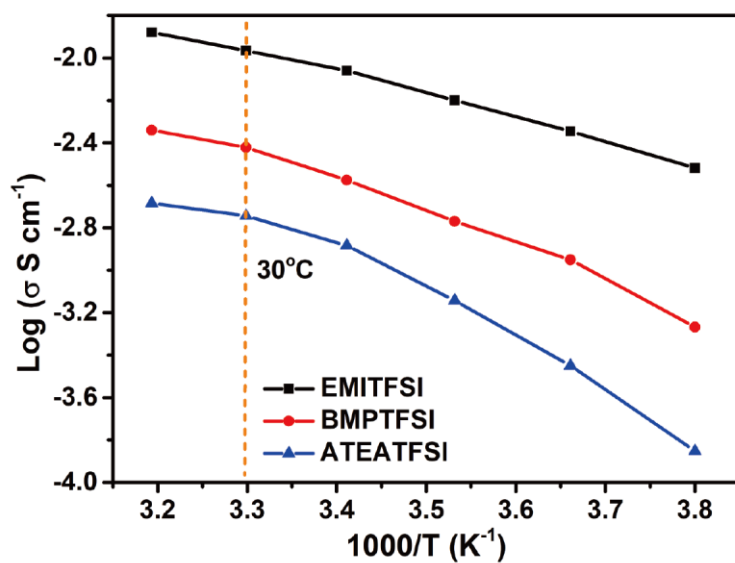
Figure S13. Ion conductivity study of different ionic liquid electrolytes, related to Figure 3.
The ionic conductivity profiles of different pure ion liquid electrolytes (EMITFSI, BMPTFSI, and ATEATFSI) at temperature from 40ºC to –10ºC. Among the three kinds of ion liquids, EMITFSI showed the highest ionic conductivity, which was about one order of magnitude higher than that of ATEATFSI. This could explain the battery performance difference shown in Figure S10 and why we chose EMITFSI as the representative pure ion liquid electrolyte to demonstrate our metal-free battery concept.
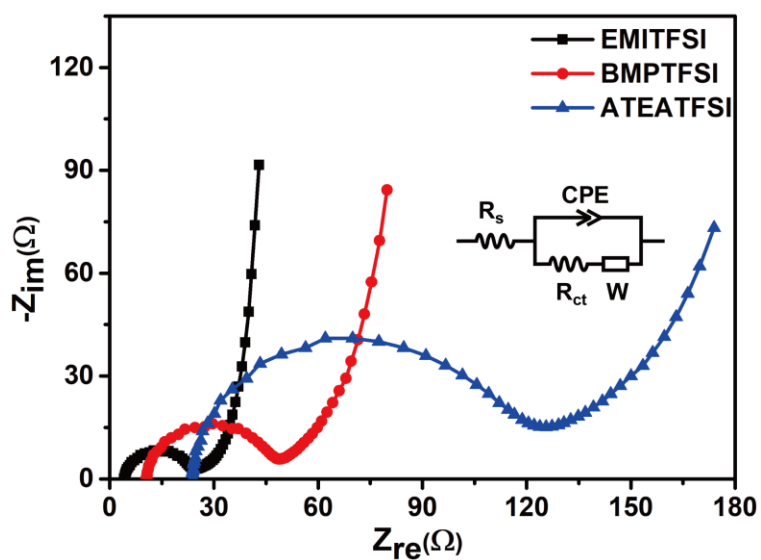
Figure S14. Impedance study of PI5/PTPAn full-cell, related to Figure 3.

Nyquist plots of the PI5/PTPAn full-cell with different pure ion liquid electrolytes after the 10th discharge process and the corresponding equivalent circuit pattern. As EMITFSI was replaced by BMPTFSI and ATEATFSI, the R_s was obviously increased from 4.09 Ω to 10.3 Ω and 22.9 Ω, while the R_{ct} was increased from 18.9 Ω to 34.4 Ω and 91.4 Ω. This tendency was quite consisted with the battery performance shown in Figure S10 and the ionic conductivity shown in Figure S11, which could be probably ascribed to the tendency of increasing ionic radius from EMI^+ to BMP^+ and $ATEA^+$ (Fig. 1B).
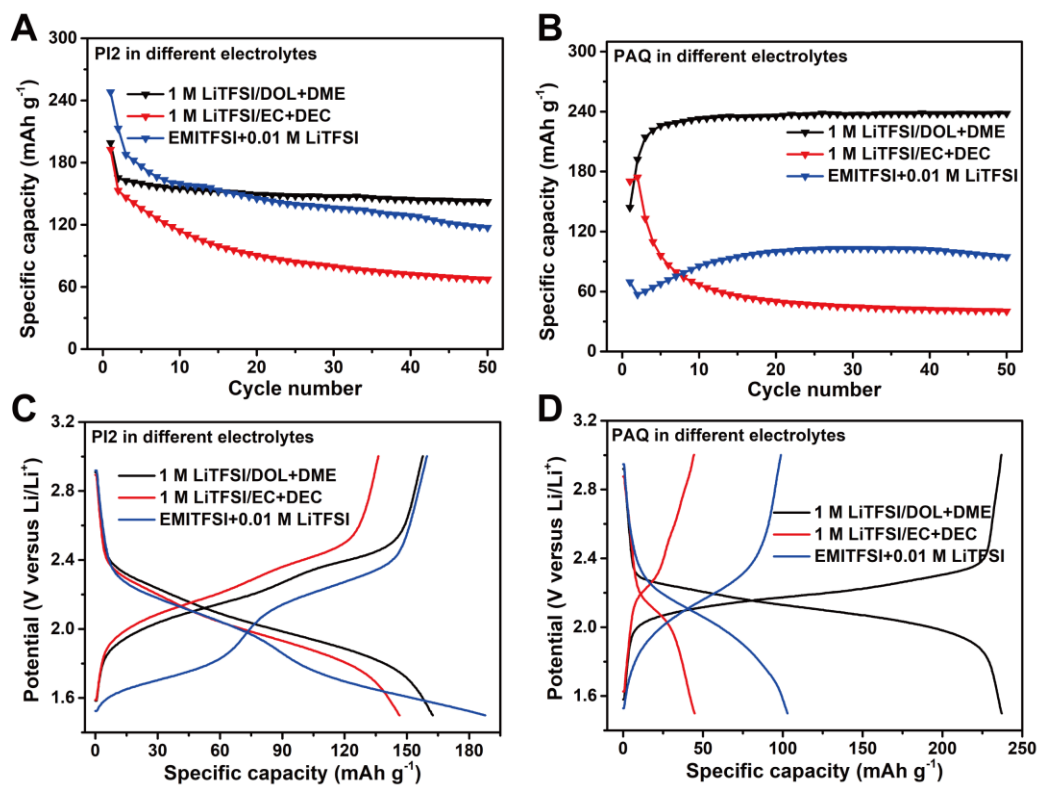
Figure S15. Results of Half-cell tests of PI2 and PAQ, related to Figure 2.

The cycling performance (A, B) and typical voltage profiles (C, from the 3rd cycle; D, from the 30th cycle) of PI2 and PAQ half-cell with different electrolytes of 1 M LiTFSI/DOL+DME, 1 M LiTFSI/EC+DEC, and EMITFSI+0.01 M LiTFSI. The results indicated that PI2 also showed high electrochemical activity in pure ion liquid electrolyte, with even lower redox potential to elevate the voltage of the full-cell, but the cycling stability needed to be significantly improved. However, the reversible capacity of PAQ was much lower in pure ion liquid electrolyte than in conventional ether electrolyte, which might be related to the poor infiltration of EMITFSI with this polymer.
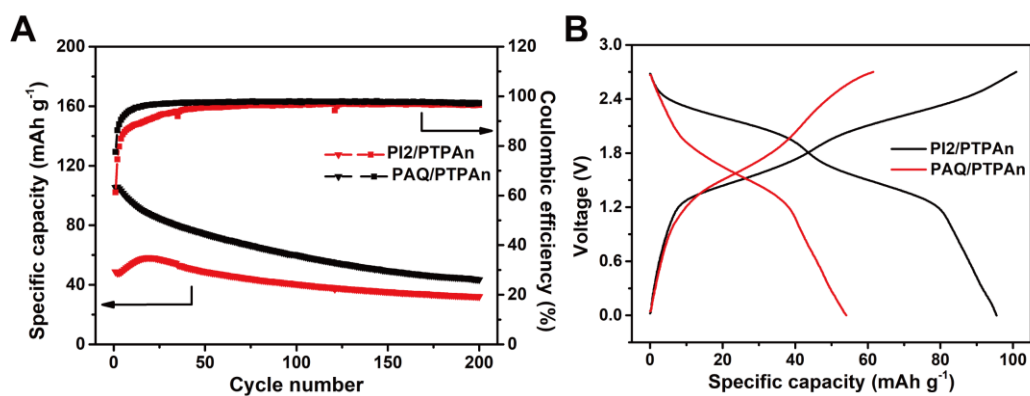
Figure S16. Study of PI2/PTPAn and PAQ/PTPAn Full-cell, related to Figure 3.

The cycling performance (A) and typical voltage profiles (B, from the 10th cycle) of PI2/PTPAn and PAQ/PTPAn full-cell with EMITFSI electrolyte. The average discharge voltage of PI2/PTPAn (1.67 V) and PAQ/PTPAn (1.40 V) were obviously improved compared to PI5/PTPAn system (1.31 V).

Table S1. Summary of the Fitted equivalent circuit from the EIS measurement of PI5/PTPAn full-cell in different status, related to Figure 3, Figure 5.

Cycles	Temperature	Electrolyte	R_s (Ω)	R_{ct} (Ω)
1st	30°C	EMITFSI	4.16	13.8
2nd	30°C	EMITFSI	4.16	16.3
10th	30°C	EMITFSI	4.09	18.9
100th	30°C	EMITFSI	4.01	23.9
10th	10°C	EMITFSI	6.29	25.3
10th	−10°C	EMITFSI	14.2	47.7
10th	30°C	BMPTFSI	10.3	33.4
10th	30°C	ATEATFSI	22.9	91.4

Table S2. Electrode information in the rate-performance test, related to Figure 3.

Electrode	Thickness	Active material loading	Total loading	Porosity
PI5	48 um	2.5 mg cm^{-2}	4.2 mg cm^{-2}	45%
PTPAn	99 um	4.2 mg cm^{-2}	7.0 mg cm^{-2}	51%

Note: the porosity of electrode was calculated according to the reference (Bülter et al., 2014).

Transparent Methods

Electrode Material Synthesis

1,4,5,8-naphthalene tetracarboxylic dianhydride (NTCDA, 98.0%, TCI), hydrazine (98.0%, J&K) were used for PI5 synthesis, and pyromellitic dianhydride (PMDA, 99.5%, J&K) and ethylene diamine (EDA, 99.0%, Sigma-Aldrich) were used for PI2 synthesis by the polycondensation reaction of equimolar dianhydride and diamine under reflux in p-chlorophenol solvent for 8 hours, the polymer products were deposited and collected from the reaction mixture after the completion of polymerization reaction following the procedure in our previous work (Song et al., 2010). PAQ was synthesized through a coupling polymerization reaction of 1,4-dichloroanthraquinone (DCAQ, 98.0%, TCI) (monomer) and bis(1,5-cyclooctadiene)nickel(0) (Ni(COD)$_2$, 98.0%, J&K) (dehalogenation agent) with the molar ratio of 10:1 in N,N-Dimethylformamide (DMF) solvent at 60°C for 5 hours according to our previous work (Song et al., 2015). All the polymers were further purified by filtration, washing with different solvent (p-chlorophenol and ethanol for PI, DMF and ethanol for PAQ) and drying in vacuum at 120°C for 12 hours. PTPAn was synthesized by chemical oxidative polymerization method using triphenylamine (TPAn, 99.0%, J&K) monomer, FeCl$_3$ (99.99%, Aldrich) oxidant with molar ratio of 1:1 in the trichloromethane (CHCl$_3$) solvent stirred for 2 hours under N$_2$ atmosphere at room temperature, after completion of the polymerization reaction, the polymer product was deposited from the mixed solvent with additional ethanol. For further purifying the PTPAn, the collected product was re-dissolved in CHCl$_3$, filtrated for removing the insoluble residues, and then concentrated, re-precipitated with acetone solution, and finally filtered, dried in vacuum at 50°C for 12 hours (Deng et al., 2013).

Electrolyte Preparation

All the electrolytes were made in argon filled glove box by mixing the electrolyte salt and solvent in fixed proportion. The salt included lithium bis(trifluoromethanesulfonyl)imide (LiTFSI, 99.9%, J&K), lithium hexafluorophosphate (LiPF$_6$, 99.99%, Aldrich), and the solvent was ethylene carbonate (EC, 99.0%, TCI), diethyl carbonate (DEC, 99.5%, J&K), 1,3-dioxacyclopentane (DOL, 99.8%, J&K), and 1,2-dimethoxyethane (DME, 99.5%, J&K). Conventional electrolyte recipe of 1M LiTFSI/EC+DEC or 1M LiPF$_6$/DOL+DME (volume ratio of the binary solvent was 1:1) was used in the study. All the ionic liquids, including 1-ethyl-3-methylimidazolium bis(trifluoromethylsulfonyl)imide (EMITFSI, 99.0%, J&K), 1-butyl-1-methylpyrrolidinium bis(trifluoromethylsulfonyl)imide (BMPTFSI, 99.0%, J&K), and amyltriethylammonium bis(trifluoromethanesulfonyl)imide (ATEATFSI, 98.0%, TCI) were commercially purchased and used as electrolyte without further purification.

Material Characterizations

Viscosity measurement was done on Brookfield DV-II+ Pro viscometer. Fourier transform infrared spectroscopy (FTIR) of the above polymer materials were conducted using KBr pellets on a NICOLET 5700 FTIR spectrometer within wave number range of 400–4000 cm^{-1} (Figure S2). X-ray photoelectron spectroscopy (XPS) measurement of the electrode in different states was carried

out on an ESCALAB 250Xi spectrometer (Thermo Fisher) equipped with a monochromatized Al Kα source (1486.6 eV) for excitation.

Electrochemical Measurements

The cathode or anode was composed of 60 wt% active material (PTPAn, PI5, PI2, PAQ), 30 wt% Ketjenblack ECP-600JD carbon and 10 wt% polytetrafluroethylene (PTFE) binder. The mixture was pressed under 15 Mpa on a disk of stainless steel mesh with typical active material loading of 0.7–1.2 mg cm^{-2} for anode (PI5, PI2, PAQ) or 1.2–2.0 mg cm^{-2} for cathode (PTPAn). CR2016 coin-cell was used in the half-cell with conventional electrolytes of 1 M LiTFSI/EC+DEC, 1 M LiPF$_6$/EC+DEC, or 1 M LiTFSI/DOL+DME, and it contained the fore-mentioned electrode as cathode and lithium anode, separated by a Celgard 2400 separator. Swagelok three-electrode cells was used in the study of the electrochemical property of the organic electrode in ionic liquid electrolyte. EMITFSI+0.01 M LiTFSI was the electrolyte and a piece of Whatman GF/D glass fiber acted as the separator. PTPAn or PI5, PI2, PAQ was the working electrode and the counter electrode was PI5 or PTPAn as required, more detailed electrode information could be found in the relative discussion. lithium foil was the reference electrode. CR2016 coin-cell was also used in the full-cell tests. It consisted of PTPAn cathode, PI5, PI2, or PAQ anode as required and pure ionic liquid electrolyte (EMITFSI, BMPTFSI, or ATEATFSI). The mass ratio of cathode to anode was determined by the rule of anode having 10% excess capacity, and the cathode and anode was separated by a disc of glass fiber. The galvanostatic charge/discharge tests were carried out on LANHE CT2001A battery test system (Wuhan, China) or Autolab PGSTAT302 electrochemical workstation (for high current rate tests). The cyclic voltammetry (CV) tests were performed on CHI660A electrochemical workstation using the above three-electrode cells. Different cutoff voltages were used depending on the cell configuration. More specifically, the voltage limit was 1.5–3.5 V for Li/PI5, 1.5–3.0 V for Li/PI2 and Li/PAQ, 3.0–4.2 V for Li/PTPAn, and 0–2.7 V for all full-cells (PI5/PTPAn, PI2/PTPAn, PAQ/PTPAn). It should be pointed out that, when testing the three-electrode cell containing EMITFSI+0.01 M LiTFSI electrolyte, the actual potential of Li$^+$/Li reference electrode is approximately 0.12 V lower than the standard Li$^+$/Li electrode potential (–3.04 V vs. SHE) according to the Nernst equation, $\Delta\varphi_{Li+/Li} = \varphi_{Li+/Li}-\varphi^{\ominus}_{Li+/Li} = (RT)/(nF)\ln[Li^+]/[Li] = -0.12$ V (T = 303.15 K, [Li$^+$] = 0.01 M). Thus, to keep the voltage consistency, the voltage range was adjusted accordingly (e.g., 1.38–3.38 V for Li/PI5, and 2.88–4.08 V for Li/PTPAn when using EMITFSI+0.01 M LiTFSI electrolyte). In addition, for the convenience of comparison, the CV or voltage profiles were all plotted versus standard Li$^+$/Li electrode. The current rate was determined by the theoretical capacity of the electrode material, such as 1C rate is 203 mA g^{-1} for PI5, and so on, 221 mA g^{-1} for PI2, 260 mA g^{-1} for PAQ, and 111 mA g^{-1} for PTPAn. The electrochemical impedance spectroscopy (EIS) of full-cells was collected at different state on Autolab PGSTAT302 electrochemical workstation with frequency range of 10^5–10^{-2} Hz and potential amplitude of 10 mV. Unless specified, all the cells were fabricated in an argon filled glove box and tested at room temperature of 30ºC.

Other Measurements

The dependence of ionic conductivity on temperature of electrolytes was measured on Leichi DDB

303A conductivity meter (Shanghai, China) from -10°C to 40°C. The flammability of the electrolytes was evaluated by the combustion experiment following the protocol in the reference (Guerfi et al., 2010; Wu et al., 2015). A piece of Whatman GF/B glass fiber soaked with 0.3 mL electrolyte was ignited and pictures were taken after different time interval to record the burning process.

Supplemental References

Song, Z., Qian, Y., Gordin, M. L., Tang, D., Xu, T., Otani, M., Zhan, H., Zhou, H., and Wang, D. (2015). Polyanthraquinone as a reliable organic electrode for stable and fast lithium storage. Angew. Chem. Int. Ed. *127*, 14153-14157.

Bülter, H., Peters, F., Schwenzel, J., and Wittstock, G. (2014). Spatiotemporal Changes of the Solid Electrolyte Interphase in Lithium-Ion Batteries Detected by Scanning Electrochemical Microscopy. Angew. Chem. Int. Ed. *53*, 10531-10535.